Introducing furanocoumarin biosynthetic genes in tomato results in coumarins accumulation and impacts growth

Alexandre Bouillé[1], Cloé Villard[1], Gianni Galati[1], Marwa Roumani[1], Aude Fauvet[1], Jérémy Grosjean[1], Lennart Hoengenaert[2,3], Wout Boerjan[2,3], John Ralph[4,5], Frédérique Hilliou[6], Christophe Robin[1], Alain Hehn[1], Romain Larbat[7*]

Corresponding author*
Phone contact: +33 (0)2 41 20 44 03

1- Université de Lorraine, INRAE, LAE, 54000 Nancy, FR
2- Department of Plant Biotechnology and Bioinformatics, Ghent University, Ghent, BE
3- Center for Plant Systems Biology, VIB, Ghent, BE
4- Department of Biochemistry, University of Wisconsin, Madison, WI 53706, USA
5- Department of Energy Great Lakes Bioenergy Research Center, The Wisconsin Energy Institute, University of Wisconsin, Madison, WI 53726, USA
6- INRAe, Institut Sophia Agrobiotech, Université Côte D'Azur, CNRS, Sophia Antipolis, France
7- Institut Agro, University of Angers, INRAE, IRHS, SFR QUASAV, F-49000 Angers, FR

#scopoletin #coumarins #furanocoumarins #tomato plant #growth #psoralen #specialized metabolism

Graphical abstract

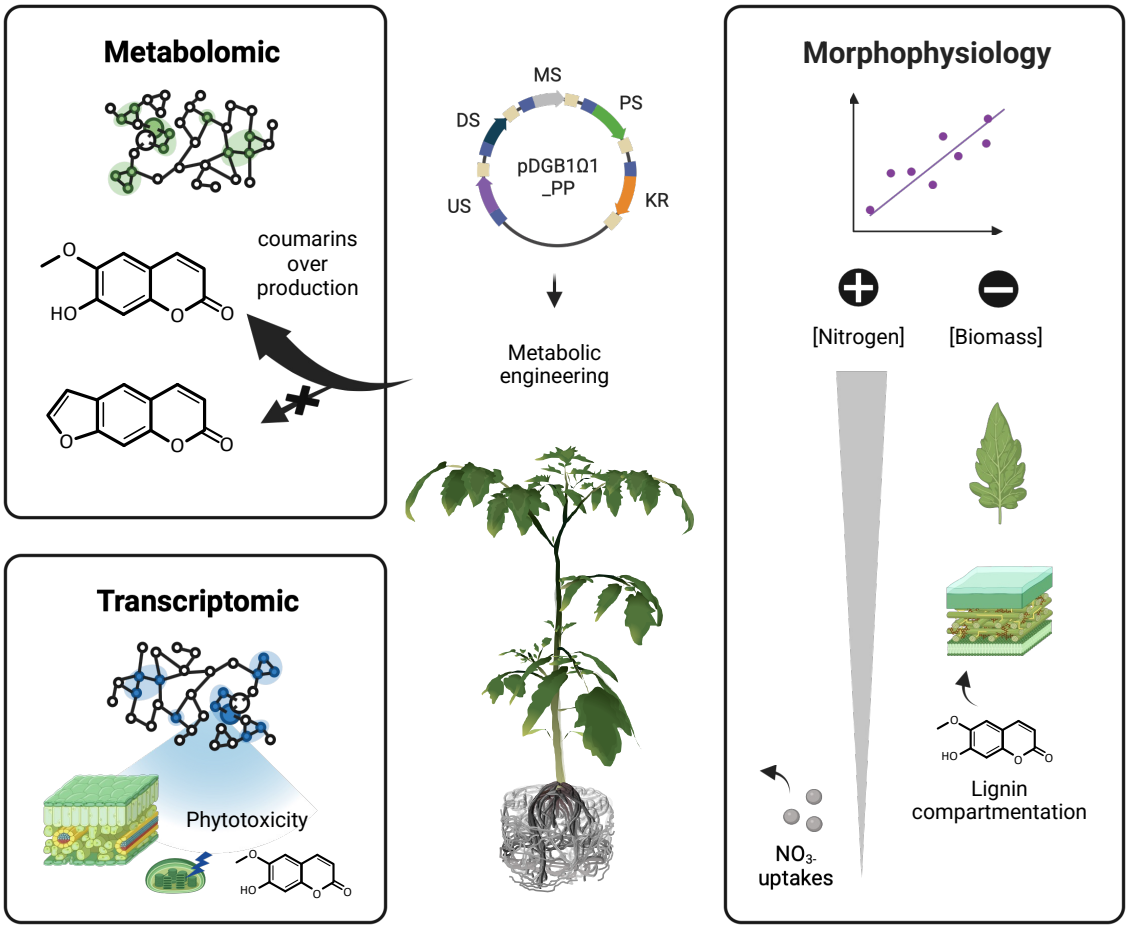

Abstract

Over the past three decades, efforts to decipher plant metabolism have shed light on key enzymes driving specialized metabolite biosynthesis. Although only few pathways have been completely investigated to date, their characterization paves the way for exploring the potential effects of specialized metabolites on plant physiology. Among them is the linear furanocoumarin pathway, which was recently completed to produce up to psoralen. In this study, we report the first metabolic engineering of the linear furanocoumarin pathway to enable artificial psoralen production in tomato, through the integration of four genes coding for the enzymes: Umbelliferone Synthase, Demethylsuberosin Synthase, Marmesin Synthase and Psoralen Synthase. Interestingly, coumarins were produced instead of furanocoumarins. Using morphophysiological, metabolomic, and transcriptomic analyses, we suggest how coumarins, particularly scopoletin, can impact growth and affect plant physiology, even at low concentrations.

As coumarins have increasingly attracted interest for agricultural applications due to their minimal environmental impact, this work both expands and challenges their potential by highlighting the physiological costs and benefits they may impose on tomato.

1. Introduction

The around 400 million years of evolution since the terrestrialization of plants have driven the emergence of numerous mechanisms for interacting with an ever-evolving environment (Morris *et al.,* 2018). The production of specialized metabolites is a key example of such adaptation as many of these compound play vital roles in enabling plants to cope with biotic and abiotic stresses (Maeda & Fernie, 2021; Weng *et al.,* 2021). Investment of resources and energy in processes that promote plant defense, particularly the biosynthesis of specialized metabolites, may come at the expense of processes that support plant growth (He *et al.,* 2022). Plants must therefore balance the trade-off between investing in the costly biosynthesis of specialized metabolites and allocating resources for growth (Neilson *et al.,* 2013).

Land plants produce a wide range of specialized metabolites (Chassagne *et al.,* 2019). Among them, linear furanocoumarins are defensive metabolites restricted to certain lineages (Sarker & Nahar, 2017). Its pathway has been largely elucidated over the past two decades, particularly in Apiaceae and Moraceae (**Fig. 1**) (Bouillé et al., 2025). Furanocoumarins are derived from the ubiquitous coumarin umbelliferone, which itself is derived from *p*-coumaroyl-CoA (Vialart *et al.,* 2012; Roselli *et al.,* 2017). The biosynthesis of linear furanocoumarins then starts with the C6-prenylation of umbelliferone to produce demethylsuberosin by a prenyltransferase (Karamat *et al.,* 2014; Munakata *et al.,* 2016). Demethylsuberosin is then cyclized by marmesin synthase, a cytochrome P450 (P450), into marmesin (Villard *et al.,* 2021; K. Wang *et al.,* 2024), which is subsequently converted to psoralen via C7-decarboxylation through *syn*-elimination of acetone by psoralen synthase, another P450 (Jian *et al.,* 2020; Larbat *et al.,* 2007, 2009). The psoralen backbone can then be hydroxylated at C5 or C8 by additional P450s to yield bergaptol or xanthotoxol, respectively (**Fig. 1**) (Krieger *et al.,* 2018; Ji *et al.,* 2024). These structures can be further decorated by other enzymes, such as *O*-methyltransferases, *O*-prenyltransferases and/or other P450s, to generate more complex

alkylated structures (Hehmann *et al.,* 2004; Zhao *et al.,* 2016; Han *et al.,* 2023; Bouillé *et al.,* 2025). Along with some of its derivatives, psoralen exhibits a broad spectrum of defensive effects, mainly driven by its ability to form covalent bonds with nucleic acids (*i.e.,* via photocycloaddition) and to alter herbivore defences (*e.g.,* through cytochrome P450 inhibition) (Neal & Wu, 1994; Kitamura *et al.,* 2005). For such reasons, psoralen is considered the first toxic metabolite in the linear furanocoumarin pathway.

In this study, we aimed to investigate the potential physiological and growth-related costs associated with the production of a novel specialized metabolite in plants using metabolic engineering. Considering the importance of psoralen in plant-environment interactions and the unknown costs its biosynthesis may impose on plants, we chosen to investigate the recently completed psoralen pathway. In that regard, using the GoldenBraid multigenic assembly system (Sarrion-Perdigones *et al.,* 2013), we integrated four linear furanocoumarin biosynthetic genes into the tomato genome (*Solanum lycopersicum*, Solanaceae), a plant that does not naturally produce these compounds, to enable the conversion of the ubiquitous *p*-coumaroyl-CoA into psoralen (**Fig. 1**). Metabolic analyses of the transgenic tomato line (referred here to as “Psoralen Pathway” or PP line) confirmed the detection of small quantities of psoralen, the expected product, but also highlighted larger modifications in the accumulation of other metabolite families, among them coumarins and particularly scopoletin. This modulation of the metabolic composition among PP line was accompanied by major transcriptomic changes and a significant modification in the biomass distribution. Our results shed light on the physiological costs associated with the implementation of the psoralen pathway in tomato and offer novel perspectives on the use of coumarins in agriculture.

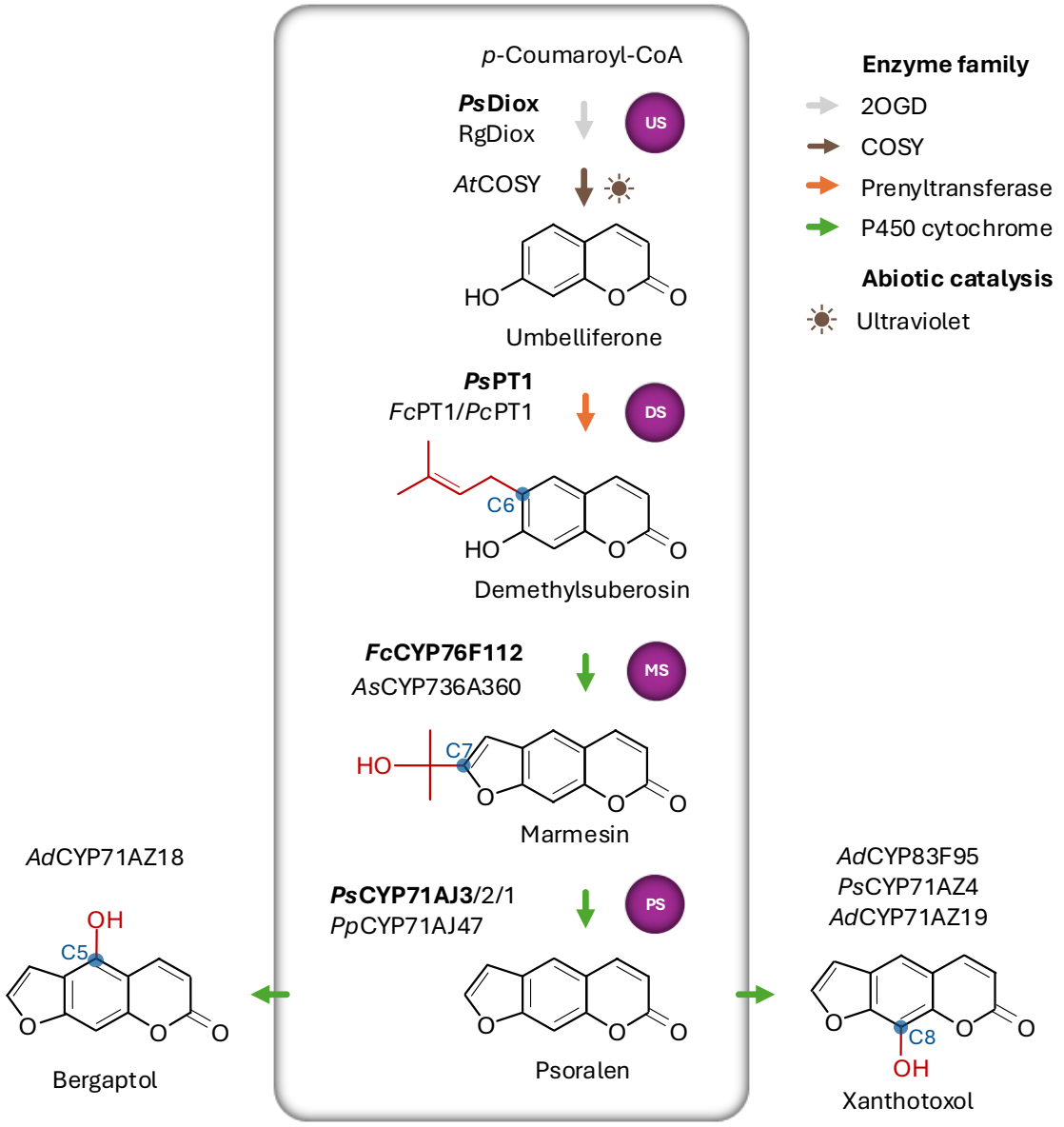

Figure 1: Simplified diagram of the psoralen pathway (PP) among linear furanocoumarin in some restricted angiosperms taxa. The pathway from *p*-coumaroyl-CoA to psoralen is framed, with the enzymes engineered in the tomato PP line encircled in purple and the specific genes inserted in the tomato genome in bold, while the carbon number on the furanocoumarin backbone is depicted in blue. Abbreviations: 2-OxoGlutarate dependent Dioxygenase (2OGD), COumarin SYnthase (COSY), PrenylTransferase (PT), CYtochrome P450s (CYP), US (*UMBELLIFERONE SYNTHASE*), DS (*DEMETHYLSUBEROSIN SYNTHASE*), MS (*MARMESIN SYNTHASE*), PS (*PSORALEN SYNTHASE*). Species: Apiaceae (*Angelica dahurica, Angelica sinensis*, *Pastinaca sativa*, *Petrolinum crispum*, *Peucedanum praeruptorum*), Rutaceae (*Ruta graveolens*), Brassicaceae (*Arabidopsis thaliana*), Moraceae (*Ficus carica*). From Larbat *et al.*, 2007, 2009; Vialart *et al.*, 2012; Karamat *et al.*, 2014; Munakata *et al.*, 2016; Roselli *et al.*, 2017; Vanholme *et al.*, 2019; Jian *et al.*, 2020; Villard *et al.*, 2021; Wang *et al.*, 2024.

2. Material and methods

2.1. Biological material and Standards

110 The tomato plants (*Solanum lycopersicum*) cultivar *West Virginia* 106 (Wva106) was used
111 as the wild-type control and for plant transformation. Analytical standards were sourced
112 from Sigma-Aldrich (Saint-Louis, MO, USA; for *p*-coumarate, scopoletin, and esculin),
113 Extrasynthese (Lyon, France; for umbelliferone, psoralen, and esculetin), TransMIT
114 (Giessen, Germany; for marmesin), Phytolab (Nantes, France; for scopolin), and R.
115 Munakata from Kyoto University (demethylsuberosin).

116 **2.2. Creation of the PP transgene**

117 The Psoralen Pathway (PP) T-DNA was created by combining the genes controlling the 4-
118 steps metabolic pathway from *p*-coumaroyl-CoA to psoralen (**Fig. 1**). The four genes were
119 *Ps*Diox (ncbi: KY081678; Roselli *et al.,* 2017) coding for Umbelliferone Synthase (US),
120 *Ps*PT1 (ncbi: KM017083; Munakata *et al.,* 2016) coding for Demethylsuberosin Synthase
121 (DS), *Fc*CYP76F112 (ncbi: MW348922 ; Villard *et al.,* 2021) coding for Marmesin Synthase
122 (MS) and *Ps*CYP71AJ3 (ncbi: C0SJS2 ; Larbat *et al.,* 2009) coding for Psoralen Synthase
123 (PS). The selection marker used in the creation of the PP transgene was the *NEOMYCIN*
124 *PHOSPHOTRANSFERASE* (*Ec*NPTII) gene conferring resistance to kanamycin, which
125 originates from the plCSL11024 vector. The coding sequence of the five genes of interest
126 were domesticated by removing internal restriction sites for *Bsa*I and *Bsm*BI, and by
127 adding flanking extensions compatible with the GoldenBraid 2.0 multigene cloning
128 system (GB2.0; Sarrion-Perdigones *et al.,* 2013). Each domesticated gene was cloned
129 into the pUPD vector using the *Bsm*BI restriction enzyme, and assembled with the *Ca*MV
130 P35S promoter (pUPD-35S, Addgene plasmid #68163) and the tNOS terminator (pUPD-
131 tNOS, Addgene plasmid #68188) to form individual transcription unit (TU). TUs were
132 assembled into the plasmid pDBGB1α1 or pDBGB1α2 by restriction/ligation using the
133 restriction enzymes *Bsa*I or *Bsm*BI, respectively, and the T4 DNA ligase, as described in
134 Sarrion-Perdigones *et al.,* 2011. The resulting TUs were further assembled two-by-two
135 into pDGB1 α- or Ω-level plasmids, through restriction/ligation, to build the final PP T-
136 DNA into pDGB1Ω1. Integrity of this final vector pDGB1Ω1_PP was validated by PCR
137 analysis (see primers section 2.3), restriction analysis (**Fig. S1a**), and sequencing of the
138 coding genes (Eco-Seq, Macrogen). PCR amplification was performed using the
139 SapphireAmp® polymerase (Takara Bio) and following the reaction cycle: Initial
140 denaturation (98 °C for 5 min), 35 cycles composed of a denaturation step (98 °C for 10

141 s), an annealing step (55 °C for 15 s) and an elongation step (72 °C for 10 s), followed by
142 a final elongation step (72 °C for 1 min). Restriction of 1µg of plasmid DNA was performed
143 using *Bsa*I, *Bsm*BI, *Pvu*II, and *Eco*RI enzymes with the FastDigest system (Thermo Fisher
144 Scientific), following the manufacturer's recommendations.

145 **2.3. Plant transformation and regeneration of the PP line**

146 The pDGB1Ω1_PP vector was co-transformed into *Agrobacterium tumefaciens* EHA105
147 with the replication helper vector pSOUP. The transformed cells were selected on solid
148 LB medium containing spectinomycin (100 mg/L), tetracycline (5 mg/L), and rifampicin
149 (20mg/L) (Hellens *et al.,* 2000; Sarrion-Perdigones *et al.,* 2013). A pre-culture was
150 performed overnight at 28 °C, 200 rpm, in 10 mL of LB medium with appropriate
151 antibiotics. A 50 mL culture was then started with 5 mL of the pre-culture to reach an
152 OD_{600nm} of 0.4-0.6. The culture was centrifuged for 10 min at 7000 ×g, then resuspended
153 in 40mL of sterile water and diluted to 30mL to achieve an OD_{600nm} of 0.08. Axenic
154 cotyledon fragments approximately 4mm in size were harvested from 7-day-old tomato
155 seedlings grown under controlled conditions (24 °C, 16 h/8 h light/dark cycles; 150
156 $\mu mol.m^{-2}.s^{-1}$, Fitoclima 1200, Aralab). The cotyledon fragments were cultured for 24 h at
157 24 °C in darkness before being co-incubated with the Agrobacteria solution for 30 min at
158 room temperature (gentle agitation every 5min). The fragments were then dried on axenic
159 paper and placed adaxial side up on co-cultivation medium for 48 h at 24 °C in darkness.
160 Partially transformed tissues were selected on kanamycin-enriched callus medium (150
161 mg/L) in Petri dishes (15 fragments per dish) at 24 °C (16 h/8 h light/dark cycles; 150
162 $\mu mol.m^{-2}.s^{-1}$) and subcultured weekly. After 3 months of subcultures, differentiated
163 seedlings from calli were cut and transferred to rooting medium before being acclimated
164 in soil in phytotrons (24 °C; 16 h/8 h light/dark cycles; 400 $\mu mol.m^{-2}.s^{-1}$; 70% humidity).
165 Several heterozygous descendants from the regenerated tomato line were obtained by
166 self-pollination. The insertion of the 5 transgenes into the genome was assessed by PCR
167 (**Fig. S1b**) using genomic DNA extracted with the kit following the supplier's
168 recommendations and the primers described as follow: *Ps*Diox_F:
169 CTAGTCGAAATGGCTCCATCTCC; *Ps*Diox_R: CGAAGATCCATTCCAAGCTCACATTTG;
170 *Ps*PT1_F: CTAGTCGAAATGGCTCAAACAATTATGC; *Ps*PT1_R:
171 GAAGATCCATTCCAAGCTCACCTC; *Fc*CYP76F112_F:

172 CTATTCTAGTCGAAATGGATATTTTCACCTC; *Fc*CYP76F112_R:
173 CGAAGATCCATTCCAAGCCTAATGATG; *Ps*CYP71AJ3_F:
174 CTATTCTAGTCGAAATGAAGATGCTTGAG; *Ps*CYP71AJ3_R:
175 GATCGAAGATCCATTCCAAGCTCATC; NPTII_F:
176 CAATTTACTATTCTAGTCGAAATGGTTGAACAAG; NPTII_R:
177 GAAGATCCATTCCAAGCTCAGAAGAAC. The expression of the 5 genes in each individual
178 was confirmed by RT-PCR for each tomato line (**Fig. S1c**). Total RNAs was extracted using
179 the E.Z.N.A.® HP kit (Omega Bio-Tek) instructions, treated with DNase (AMPD1-1KT,
180 Sigma) to remove genomic DNA contaminants, and then reverse-transcribed into cDNA
181 using the High-Capacity RNA-to-cDNA Kit (Applied Biosystems™), according to the
182 supplier's recommendation.

183 **2.4. Plant cultivation and measurement of morpho-physiological traits**

184 Four sets of plant cultivation and harvest were performed over a period of four months.
185 Three sets of 6-8 plants per genotype were used for transcriptomic and metabolomic
186 analyses (23 WT, 19 PP), and one additional set (23 WT, 19 PP) for morphophysiological
187 measurements, for a total of 46 WT and 38 PP plants. All plants were staggered under
188 identical conditions. The first three were used for the metabolomics and transcriptomics
189 analyses. The fourth series was dedicated to measuring morphometric traits, including
190 carbon and nitrogen allocation, and lignin composition/content in the stems. At harvest,
191 stem and petiole tissues were separated from the leaves and roots. For metabolomics
192 analyses, petioles and internodes were combined.
193 Tomato plants were grown in 1.5 L pots with 0.5 L of potting soil (Stender D400, NPK
194 14/10/18, pH 6.2, sieved to 5 mm). The climatic conditions in the growth chamber were
195 set at 24 °C with 16 h/8 h light/dark cycles, LED illumination at 400 $\mu mol.m^{-2}.s^{-1}$, and 70%
196 humidity. Plants were watered to maintain 70% soil moisture three times a week with
197 osmosed water. Weekly, tomatoes were fertilized with horticultural fertilizer (50 mL at 2
198 $g.L^{-1}$) (9:16:36 of N:P:K, MultiTec™). Tomato plants were harvested at 28 days after sowing,
199 at the vegetative stage. Roots were gently washed with a brush and untangled for length
200 measurements. For metabolomic and transcriptomic analyses, tissues were rapidly
201 snap-frozen in liquid nitrogen before being finely ground and stored at -80 °C. Leaf areas
202 without petioles were measured using a planimeter (Li-3100 C Area Meter, Li-Cor,

203 Lincoln, Nebraska, USA). Tissues used for carbon, nitrogen, nitrate and lignin content
204 measurement were dried in an oven at 70 °C for 1 week and then finely ground using an
205 orbital mill (Pulverisette 6, Fritsch, France) before being stored at room temperature in a
206 dry-preserving package. Resulting powder was used for carbon, nitrogen and lignin
207 measurements.

208 **2.5. Total nitrogen and carbon analyses**

209 Total C and N contents in dry tissues were determined using 3mg of dry matter, according
210 to the Dumas method, with an elemental auto-analyzer (Unicube, Elementar,
211 Langenselbold, Germany).

212 **2.6. Cell wall characterization**

213 Lignin and its components were quantified according to Lu *et al.,* 2021. Briefly, cell wall
214 residues (CWR) were extracted using successive boiling in solvent baths. Lignin content
215 was quantified in percentage of CWR according to the Cysteine-Assisted Sulfuric Acid
216 (CASA) method. The lignin composition of CWR was measured using the thioacidolysis
217 method as described by Rolando *et al.,* 1992, and the released fragments were analyzed
218 using GC-MS at the VIB Metabolomics Core as described in (Hoengenaert *et al.,* 2022).
219 The composition of the lignin was analyzed as described in (Hoengenaert *et al.,* 2022).
220 Briefly, 20 mg of stems CWR were cellulase-digested and resuspended in DMSO. Scans
221 of HSQC NMR spectra (Heteronuclear Single-Quantum Coherence) $^{1}H–^{13}C$ short-range
222 correlation experiments were acquired for 6h, followed by a second 54h acquisition for
223 improve sensitivity.

224 **2.7. Metabolites extraction**

225 Frozen powders from leaves, stems and roots (100 mg FW) were extracted twice using
226 maceration (16 h in the dark at 22 °C with slow vertical agitation) followed by sonication
227 (37 kHz, 10 min at room temperature), each time with 800 µL of methanol/deionized
228 water (80/20). The macerates were then centrifuged (10 min, 16100 g, 22 °C). The
229 supernatants (1.6 mL) were collected, dried (5-7 h under vacuum, Concentrator Plus,
230 Eppendorf) and then resuspended in 100 µL of methanol/deionized water (80/20). The
231 extracts were filtered (0.2 µm, Minisart® RC4 membrane, Sartorius, REF17821) and stored
232 at -20 °C. Extracts were added with taxifolin (285 µM) as an internal quantification
233 standard.

234 **2.8. Metabolomics analysis**

235 Chromatographic analyses coupled with High Resolution Mass Spectrometry were
236 performed on a Thermo Scientific Vanquish UHPLC system equipped with a binary pump,
237 an autosampler, a temperature-controlled column (40 °C) and a Diode Array Detector.
238 Extracted samples were separated on a XB-C18 Kinetex (150 × 2.1 mm, 2.6 µm)
239 (Phenomenex Inc., Torrance, CA, USA) using a gradient of mobile phase composed of
240 0.1% formic acid in water (A) and 0.1% formic acid in methanol (B) at a flow rate of 200
241 $\mu L \cdot min^{-1}$. The separation of the compounds was performed using a 30 min mobile phase
242 gradient (A: B; v/v). The elution method is as follows: (90:10) at 0 min, (90:10) up to 2 min,
243 (70:30) up to 10 min, (5:95) up to 20 min remaining 5 min, (90:10) up to 26 min. The
244 molecules are detected according to their absorbance at different wavelengths between
245 190 and 800 nm.

246 $HRMS^1$ detection was performed on an Orbitrap IDX™ (ThermoFisher Scientific, Bremen,
247 Germany) mass spectrometer in positive and negative electrospray ionization (ESI)
248 modes. The capillary voltages were set at 3.5 kV and 2.5 kV for positive and negative
249 modes, respectively. The source gases were set (in arbitrary unit min^{-1}) to 40 (sheath gas),
250 8 (auxiliary gas) and 1 (sweep gas) and the vaporizer temperature and ion transfer tube
251 was respectively 320 °C and 275 °C. Full scan MS^1 spectra were acquired from 120 to
252 1200 m/z at a resolution of 60,000. MS^2 analysis was performed on the pooled-samples
253 vial using the data dependent acquisition (DDA) mode and fragments were analyzed by
254 Orbitrap at a resolution of 15000. For this analysis, the AcquireX data acquisition
255 workflow was applied. The raw data were uploaded on the Compound discoverer 3.3
256 software (ThermoFisher Scientific, Bremen, Germany) to run the untargeted
257 metabolomics workflow (peak detection, chromatogram alignment and peak grouping in
258 features). In addition, the full MS^1–MS^2 dataset was exported as a mascot generic format
259 (mgf) file and analyzed through the Sirius 5 software (Dührkop *et al.,* 2019). Briefly, the
260 procedure implies the automatic annotation of molecular formula using SIRIUS and
261 ZODIAC (Dührkop *et al.,* 2019; Ludwig *et al.,* 2019). Then, molecular structure prediction
262 was proposed through CSI: FingerID (Hoffmann *et al.,* 2021). Finally, feature was
263 assigned to chemical families using CANOPUS (Djoumbou Feunang *et al.,* 2016; Dührkop
264 *et al.,* 2019; H. W. Kim *et al.,* 2021). Further annotation was performed using Compound

265 Discoverer 3.3 by predicting elemental composition, searching in local and public mass
266 and formula databases such as ChemSpider, HMDB, and LipidMaps, and querying
267 spectral databases including mzCloud, MoNA, and GNPS.
268 Formal identification of coumarins and furanocoumarins, was afforded via comparisons
269 with commercial standards according at least to their retention time (RT), mass (MS^1) and
270 mass fragmentation (MS^2) when available. A standard curve was established for the
271 scopoletin quantification using as internal standard the taxifolin (285 µM).

272 **2.9. Construction and analysis of RNAseq libraries**

273 Total RNA from leaves and roots was extracted from 3 plants per genotype (WT and PP)
274 as previously described (Roumani *et al.,* 2022). RNA concentrations were determined
275 from their absorbance at 260 nm. Their purity was evaluated by the 260/280 nm
276 absorbance ratio, their quality was checked by electrophoresis on a 1% agarose gel and
277 their integrity by determining and considering an RNA Integrity Number (RIN) >7 (Agilent
278 BioAnalyzer 2100). Transcript data was obtained by RNA-Seq Illumina pair-end
279 sequencing (2× 150pb) using the NovaSeq 6000 methods for 30 million read pairs. Raw
280 data were cleaned using Trimmomatic (Bolger *et al.,* 2014). The quality of the sequences
281 was assessed using FastQC. The transcripts were mapped on the tomato genome
282 (ITAG2.4) using the BWA-MEM software (Li & Durbin, 2009). Count tables were generated
283 using the FeatureCounts software (Version 1.6.4) and Samtools merge workflows (Liao *et*
284 *al.,* 2014). The differential gene expression was performed with the glmfit option within
285 the edgeR package for a FDR <0.05 (Robinson *et al.,* 2010) and using AskoR (Alves-
286 Carvalho *et al.,* 2021). We performed, within AskoR, a clustering using kmeans
287 classification algorithms (Coseq R package) (Godichon-Baggioni *et al.,* 2019). Functional
288 annotations, such as gene ontologies and interproscan features, were extracted from
289 ITAG2.4_protein_functional.gff3 file. Differentially expressed genes (DEGs) between WT
290 and PP lines DEGs were used to perform GO enrichment analysis (GOEA) restricted to
291 the Biological Processes on ShinyGO (version 0.80) using the "*Solanum lycopersicum*
292 genes SL3.0" and a FDR cutoff <0.05 (Ge *et al.,* 2020). RNA-seq dataset from tomato
293 leaves and roots is publicly available through the Data.gouv.fr repository:
294 https://doi.org/10.57745/G2Z4VV.

295 The results of the RNAseq differential analysis were confirmed by following the
296 expression level of 2 genes (*Sl*COSY and *Sl*PRCA) in addition to the 5 engineered genes in
297 leaves and roots of the PP and control tomato plants. The list of targeted genes and
298 primers used is given in **Table S2h**. The expression level was followed by RT-qPCR. For
299 that purpose, a total of 200 ng of DNA-free RNA samples was reverse transcribed in a final
300 volume of 20 µL using the RNA to cDNA kit (Life technologies, Tokyo, Japan). cDNAs were
301 then diluted 10 times. Gene expression was measured by qPCR on a CFX Duet Realtime
302 PCR System (Bio-Rad). Each PCR reaction was made in 20 µL containing primer pairs at
303 0.3 µM, 40 ng of cDNAs in 1× Mesa Blue Premix (Eurogentec) and followed the
304 amplification protocol consisting in a denaturing step at 95 °C for 30 s, 40 cycles at 95 °C
305 for 5 s and 60 °C for 30 s. The gene expression of each sample was calculated with three
306 analytical replicates and normalized to the two internal control genes *ACT* and *GAPDH*.

307 **2.10. Statistical Analysis**

308 Measured and calculated morphometric and physiological variables, as well as relative
309 and absolute quantified metabolites were statistically analyzed by comparing WT and PP
310 lines using a non-parametric Kruskal-Wallis test.

311

312 **3. Results**

313 **3.1. The PP line regeneration**

314 To insert the Psoralen Pathway (PP) in tomato plants, we first leveraged the GoldenBraid
315 technology to assemble the selected four genes encoding the enzymes required for the
316 conversion of *p*-coumaroyl-CoA into psoralen. The T-DNA was build-up with 5 genes
317 organized as transcription units (TUs) (Larbat *et al.,* 2009; Munakata *et al.,* 2016; Roselli
318 *et al.,* 2017; Villard *et al.,* 2021), each independently under the control of the constitutive
319 *CaMV*35S promoter and the tNOS terminator (**Fig. 1**; **Fig. S1**). Then, we integrate the PP
320 T-DNA into the genome of the *Wva*106 tomato cultivar using an *agrobacterium*-mediated
321 stable transfection. Plant selection was allowed by a fifth similarly assembled TU
322 including the kanamycin resistance. By assessing genomic integration via PCR on gDNA,
323 we successfully regenerated two independently transfected lines (**Fig. S1b**). Among the
324 two lines, qPCR revealed that only one line (the PP line) showed a constitutively high
325 expression levels of each transgene in the investigated leaves and roots, compared to the

326 WT (**Table S2g,h; Fig. S1c**). Our study focused on this particular line, which exhibited a
327 phenotype similar to the WT (**Fig. S1e**).
328
329 **3.2. The PP line accumulates coumarins**
330 To investigate the impact of Psoralen Pathway integration on tomato plant metabolic
331 composition, we compared the metabolomes of PP and WT plants in leaves, stems, and
332 roots using untargeted LC-HRMS analysis of hydro-methanolic extracts. To strengthen
333 the analysis, given that only one PP line was obtained, we performed three independent
334 cultivation rounds under identical growing conditions, resulting in 23 WT and 19 PP
335 plants. The metabolome comparison between PP and WT in all the three-round
336 cultivation of plants and across the three organs, highlighted an overall tendency to a
337 higher accumulation of dozens to hundred metabolic features in the PP line. By
338 considering only significant metabolic features that differentially accumulated
339 (Benjamini-Hochberg $p<0.05$), 82 metabolic features across leaves, stems and roots
340 were retained (**Table S1**). One metabolic feature was less abundant in the PP line
341 whereas all others were enriched in comparison to the WT. Putative annotation of these
342 features allowed to categorize 20 of them as fatty acids and 19 as phenylpropanoids (*i.e.,*
343 10 coumarins, 7 phenolamides, the furanocoumarin: psoralen, and one miscellaneous
344 compound) (**Fig. 2a**). The abundance of only eight of the metabolic features were
345 significantly affected in at least two organs, and among them scopoletin, the only
346 metabolite that was found to be differential in leaves, stems and roots (**Fig. 2b**).
347

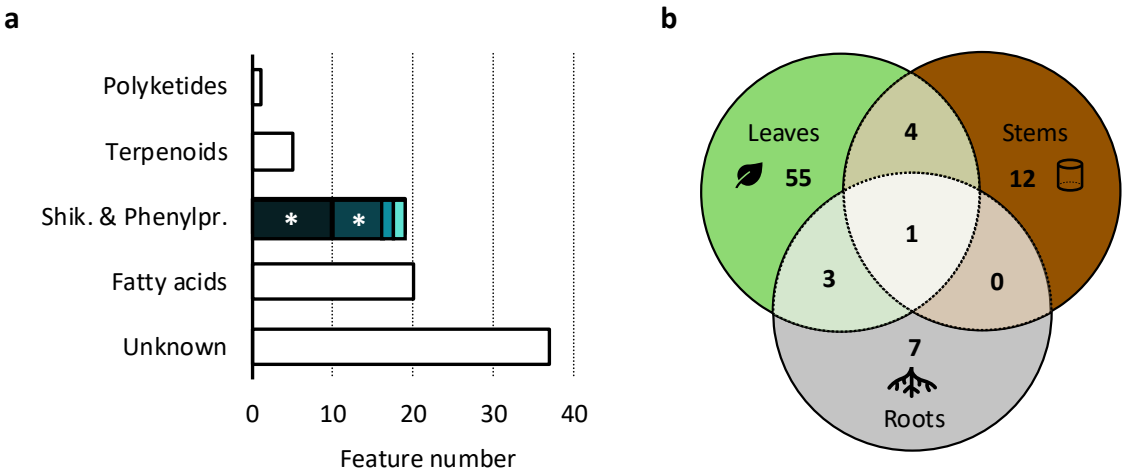

Figure 2: Untargeted comparative metabolomic profiling of the Psoralen Pathway (PP) and the Wild-Type (WT) tomato lines. (**a**) Number of metabolic features significantly over-accumulated in the PP line compared to the WT. Metabolic features are categorized according to the NP-Classifier ontology (Kim *et al.,* 2021). Shikimate and phenylpropanoids are highlighted in blue from dark to light: coumarins*, phenolamides*, others, furanocoumarins. Asterisks* correspond to metabolic subclasses significantly enriched (**Table S1b**). (**b**) Venn diagram describing the distribution of the PP line's over-accumulated features across leaves (green), stems (brown) and roots (grey) compared to the control line. Number of replicates for leaves, stems, roots: WT (n=23), PP (n=19). The data are based on 3 independent cultivation rounds of tomato plants grown in the same phytotronic conditions.

We then performed targeted analyses focusing on coumarins and metabolites of the psoralen pathway. Psoralen and its precursors (*i.e.,* demethylsuberosin and marmesin) were detected only in trace amounts across the analyzed organs of the PP line, and were absent from the WT (**Fig. 3a**). The PP line exhibited significant increases in *p*-coumaric acid and umbelliferone levels in the leaves (50- and 31-fold, respectively in comparison to WT), with no significant changes in other plant parts. Scopoletin concentrations were significantly increased in all organs of the PP line (23- to 1799-fold), and especially in stems where it reached concentrations close to 5 µg/g of DW (**Fig. 3b**). Esculetin and its glycoside form esculin accumulated significantly higher in the PP line than in the WT (**Fig. 3a**). On the opposite, scopolin accumulation was not different between the WT and the PP line.

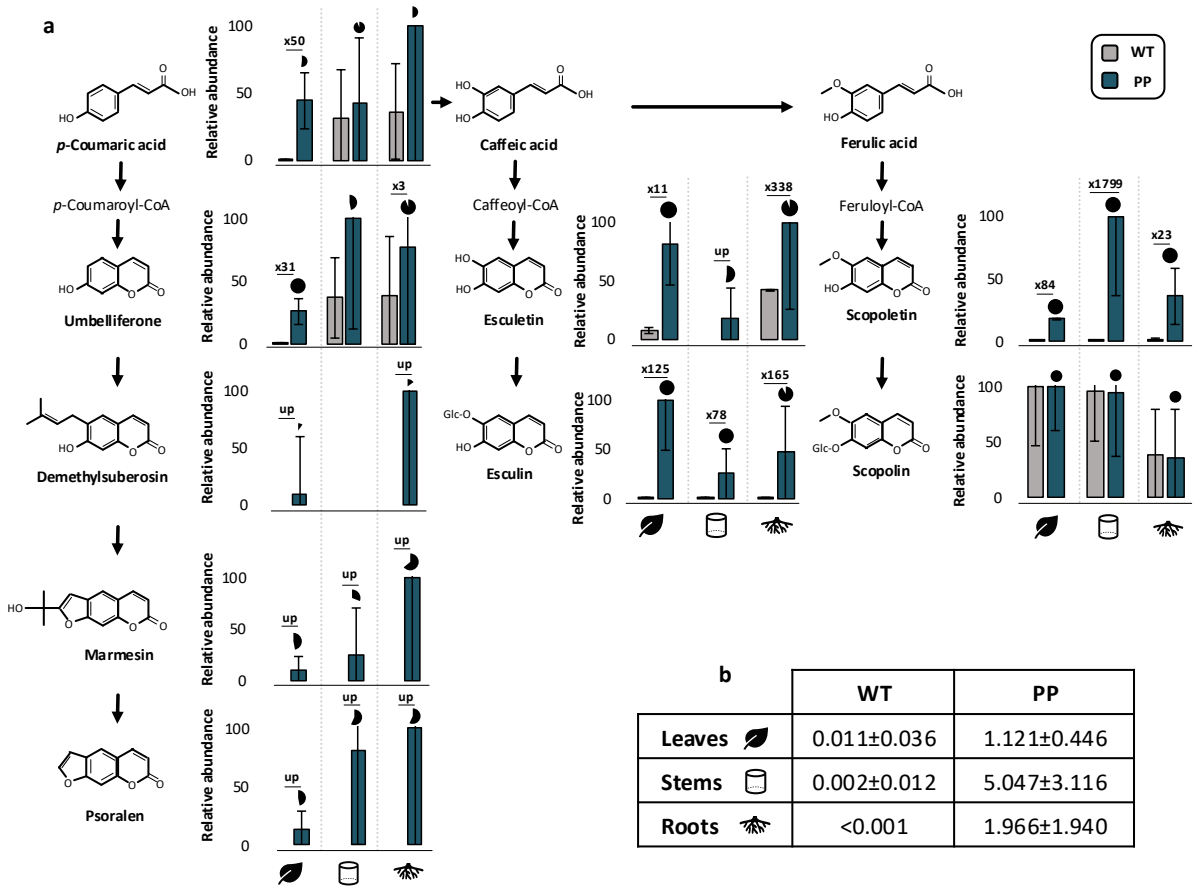

b

	WT	PP
Leaves	0.011±0.036	1.121±0.446
Stems	0.002±0.012	5.047±3.116
Roots	<0.001	1.966±1.940

Figure 3: Comparative targeted profiling of coumarins and furanocoumarins in the Psoralen Pathway (PP) and the Wild-Type (WT) tomato lines. (**a**) Relative accumulation of reported coumarins and furanocoumarins in the PP line (blue) versus the WT line (grey), expressed as mean ± standard deviation. Percentage of replicates containing the metabolite in the PP line is illustrated using black pie charts. Only significantly differentially accumulated metabolites, assessed by the Kruskal-Wallis test ($p<0.05$*), are depicted according to their increasing fold change in the PP line compared to the WT line. 'Up' refers to compounds detected only in the PP line. (**b**) Absolute quantification of scopoletin in µg/g of dry weight. Data are expressed as percentages (a) or absolute quantity for each metabolite relative to the most abundant peak area, normalized to the internal standard taxifolin, and reported per mg of dry weight; Number of replicates for leaves, stems, roots: WT (n=23), PP (n=19). The data are based on 3 independent cultivation rounds of tomato plants grown in the same phytotronic conditions.

3.3. Scopoletin is released by a lignin-degradative method

Scopoletin has recently been described to be able to incorporate into the lignin polymer of *Arabidopsis thaliana* (Brassicaceae) and *Populus sp* (Salicaceae) transgenic lines producing this metabolite in the stems (Hoengenaert *et al.,* 2022; N. Wang *et al.,* 2025). Accordingly, the lignin composition was analyzed in the PP line and compared to that in the WT. Lignin content (**Fig. 4a**) and composition (H, G, S) (**Fig. 4b-c**) in the stems of the PP line were not significantly affected compared to WT. However, analysis of the

393 thioacidolysis released monomers indicated a slight but significant increase in the
394 release of scopoletin in the PP line (2.8×) compared to the WT line (**Fig. 4c**), suggesting
395 the presence of scopoletin in the cell wall as well as in the lignin.
396

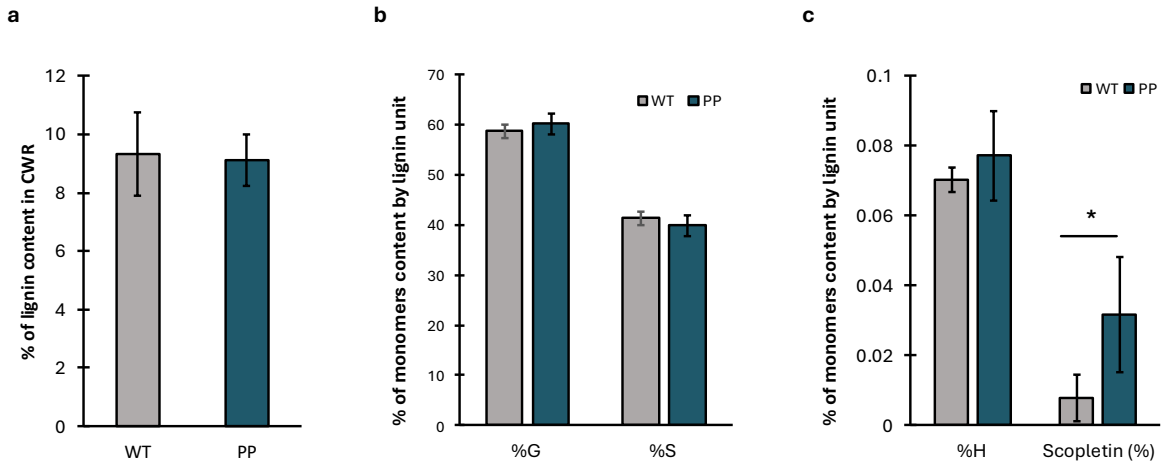

397

398 **Figure 4: Impact of the Psoralen Pathway (PP) line on lignin content (a) and composition for**
399 **G, S (b), and H monomers, as well as for scopoletin (c), in stems compared to the Wild-Type**
400 **(WT) line.** The average percentage of monomers and scopoletin are calculated based on the
401 content of H, G, and S units and scopoletin in the lignin. The error bars indicate the standard
402 deviation. The lignin content was measured as percentage of Cell Wall Residue (CWR) using the
403 Cysteine-Assisted Sulfuric Acid (CASA) method (Lu *et al.,* 2021). Data were compared using the
404 Kruskal-Wallis's test (p-value<0.05) (p-value for scopoletin % = 0.00106); WT (n=8) and PP (n=9).
405

406 **3.4. Specific genes regulation in the PP line**

407 To further understand the metabolic changes observed in the PP line, we then
408 investigated its transcriptome compared to the WT. Results highlighted 1014 and 53
409 differentially expressed genes (DEGs) in the leaves and roots, respectively, of the PP line
410 (**Fig. 5a; Table S2**). In leaves, the 1014 DEGs comprised 659 upregulated and 355
411 downregulated genes in the PP line compared to WT. In roots, 41 genes were upregulated
412 and 12 downregulated. Seventeen DEGs were common to leaves and roots. Gene
413 Ontology Enrichment Analysis (GOEA) was performed on the up- and downregulated
414 DEGs identified. In leaves, GOEA analysis highlighted an overall upregulation of genes
415 involved in processes related to response to stress and wounding (**Fig. 5b**), whereas the
416 main trend was a downregulation of genes associated to chlorophyll biosynthesis (**Fig.**
417 **5c**). In roots, the relatively short list of DEGs did not lead to any significant enrichment
418 using GOEA.

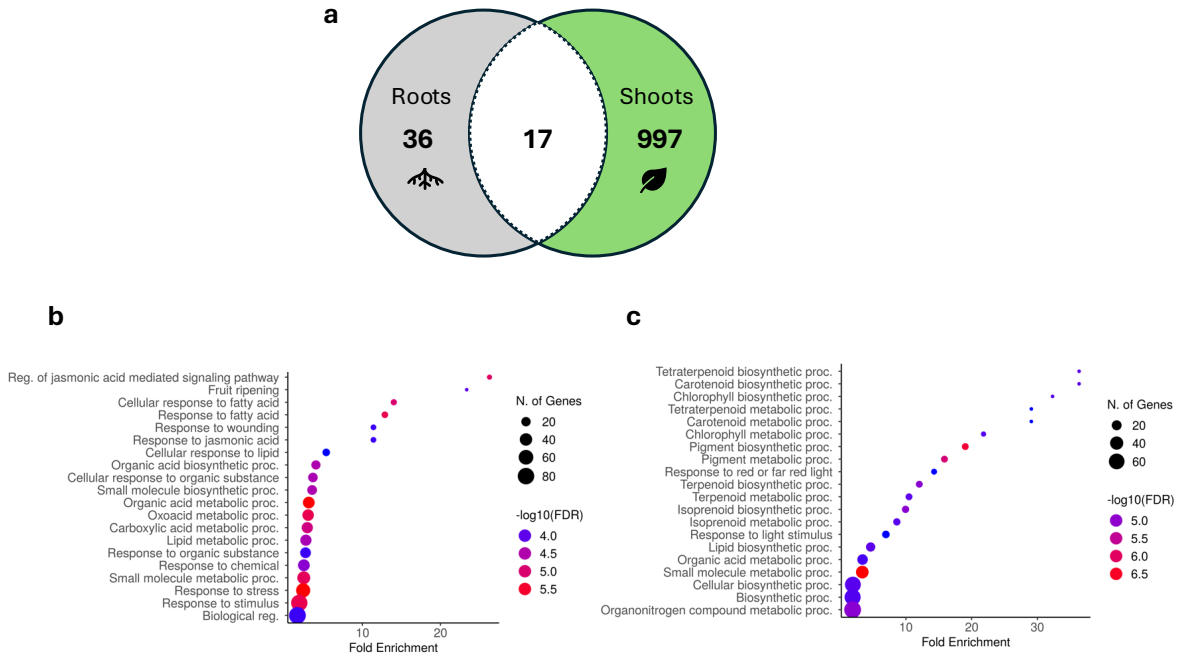

Figure 5: Transcriptomic regulation in the Psoralen Pathway (PP) line compared to the Wild-Type (WT) line. (**a**) Differentially Expressed Genes (DEGs) in leaves and/or roots (FDR<0.05). Gene Ontology Enrichment Analysis (GOEA) on biological processes for (**b**) upregulated and (**c**) downregulated genes considering only leaves (False Discovery Rate: FDR<0.05). The position of the circles represents the fold change by related to the ratio PP/WT. The size of the circles represents the number of Differentially Expressed Genes (DEGs) in each Gene Ontology (GO) category. The color of the circles indicates the statistical significance. The data consist of 3 replicates of PP and WT per tissue.

Using a differential gene analysis based on 3 replicates in leaves and roots comparing the PP and WT lines, we highlighted only strongly DEGs in the PP line (**Fig. 5**). Finer regulatory patterns were uncovered through a K-means clustering approach, which revealed 11 expression clusters based on gene expression profiles in leaves and roots, comparing the PP and WT lines (**Fig. S2**). Among them, five clusters displayed expression patterns that distinguished the PP line from the WT. The smaller and most specific expression cluster was cluster 8 regrouping 309 genes with a higher expression in both the leaves and roots of the PP line in comparison to WT. In addition, cluster 2 (1449 genes) contained genes specifically over-expressed in the roots of the PP line, and cluster 7 (1113 genes), over-expressed genes in the leaves. Conversely, the clusters 1 (743 genes) and 5 (1466 genes) grouped genes downregulated in leaves and roots of the PP line compared to the WT. GOEA of cluster 8 indicates the induced expression of genes potentially linked to the PP

line's response to stress, likely signaled *via* jasmonate and in response to lipids (**Fig. 6a**). As an extension of cluster 8, the same trend was observed as for the genes from cluster 7 (upregulated in leaves of the PP line) (**Fig. 6b**). The cluster 2 (upregulated genes in roots of the PP line), were enriched in processes related to hormonal regulations (**Fig. 6c**). Among the processes related to downregulated genes (**Fig. 6d,e**), DNA replication and cell cycle appeared affected in the roots of the PP line (cluster 5), whereas lipid and sterol biosynthesis were, in leaves (cluster 1).

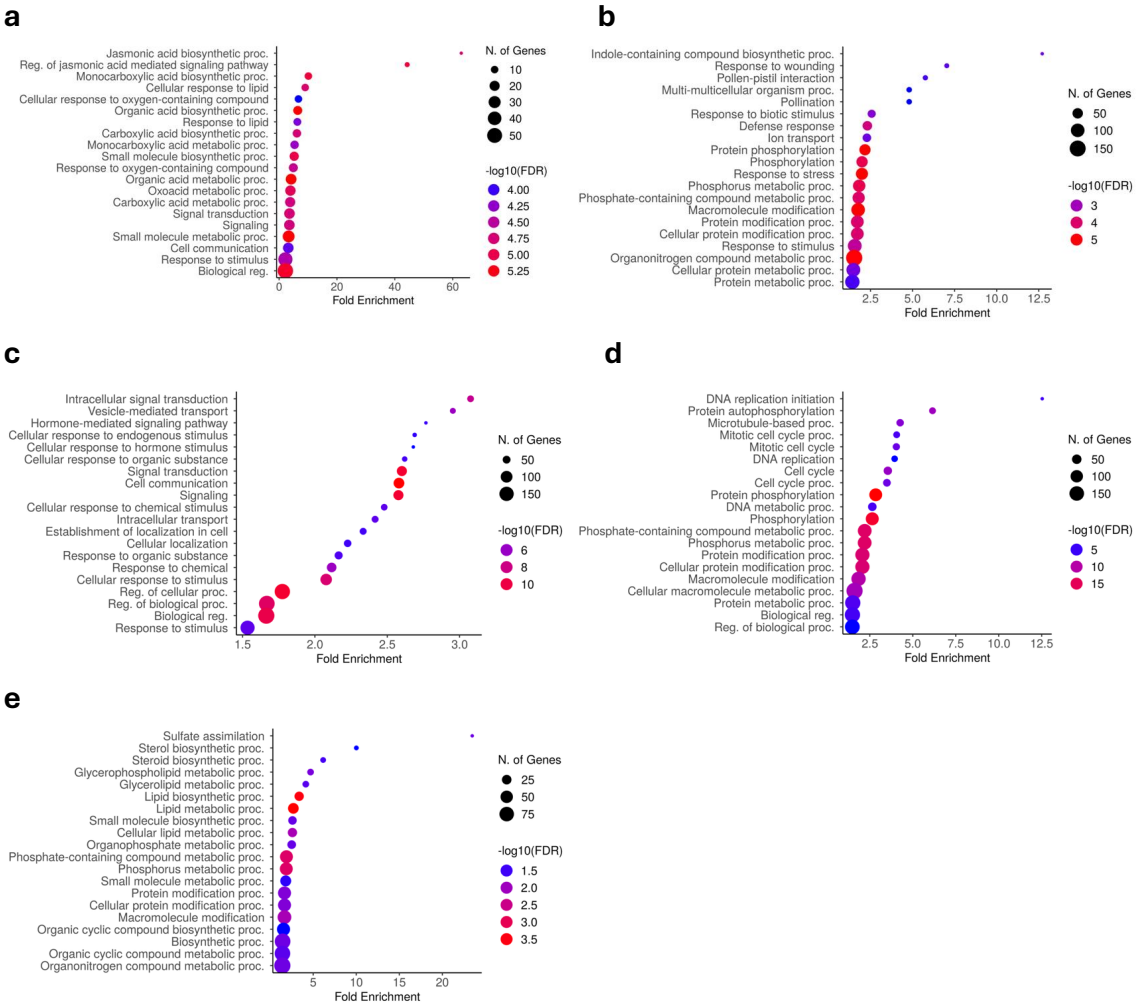

Figure 6: Gene Ontology Enrichment Analysis (GOEA) on biological processes in the Psoralen Pathway (PP) line compared to Wild-Type (WT) line for clusters 8 (a), 7 (b), 2 (c), 5 (d) and 1 (e). (*False Discovery Rate:* FDR<0.05). The position of the circles represents the fold change by related to the ratio PP/WT. The size of the circles represents the number of Differentially Expressed Genes (DEGs) in each GO category. The color of the circles indicates the statistical significance. Gene clusters were grouped using the k-means method. (**a**) Cluster 8 includes 309 upregulated genes and most of those were specifically differentially expressed in the leaves and roots of the PP line compared to the WT line (10/17 genes). (**b**) Cluster 7 contains 1113 upregulated genes in leaves. (**c**) Cluster 2 contains 1449 upregulated genes in roots. (**d**) Cluster

1 and (**e**) cluster 5 contain 743 and 1465 downregulated genes in roots and leaves, respectively. The data consist of 3 replicates of PP and WT per tissue.

3.5. The PP line showed reduced biomass and elevated nitrogen content

To identify potential impacts on the growth and development of the PP line compared to the WT line, we performed a comparative resource allocation and morphology analysis (**Table S3**). After 28 days of growth, PP and WT plants exhibited comparable morphology and size (**Fig. S1e**), with similar leaf numbers and stem lengths between days 13 and 28, indicating no significant developmental changes (**Table 1**). However, dry biomass in the PP line was significantly reduced by 21.3% compared to the WT. This decrease was uniformly distributed across plant organs with the exception of stem which had a similar amount of dry biomass compared to the WT. As a results, the resource allocation pattern in the PP line was significantly different from the WT, with a decrease in the proportion of matter in the leaves (-10%) and an increase in the stem (+20%) (**Table 1**). The decrease in the biomass accumulation in leaves was in accordance with an increase in the Specific Leaf Area (SLA) in the PP line.

	Variable	WT average ± SE	PP average ± SE	p-value
Dry weights	Foliar blades (g)	2.46 ± 0.36	1.74 ± 0.24	**0.0004***
	Petioles (g)	0.49 ± 0.07	0.4 ± 0.05	**0.0222***
	Stems (g)	1.11 ± 0.28	1.05 ± 0.17	0.4142
	Roots (g)	0.49 ± 0.05	0.39 ± 0.06	**0.0025***
	Stems/Roots ratio	8.20 ± 1.07	8.15 ± 0.70	0.9349
Tissue allocation (% by DW)	Foliar blades	54.06	48.6	**0.0042***
	Petioles	10.76	11.17	0.2529
	Stems	24.39	29.32	**0.0178***
	Roots	10.76	10.89	0.9349
Development	Stems (cm)	49.95 ± 7.42	51.33 ± 6.02	0.6532
	Roots (cm)	44.21 ± 15.1	44.22 ± 9.38	0.7439
	Leaf number	8	8	1
	D13/D28 plant height	0.1 ± 0.02	0.1 ± 0.02	0.8064

Key growth analysis parameters	Stems/Roots ratio	1.24 ± 0.43	1.2 ± 0.28	1
	SLA (cm2.g^{-1})	236.48 ± 33.67	329.73 ± 35.81	**0.0002***
	SRL (cm.g^{-1})	90.95 ± 39.82	115.21 ± 31.85	0.0724
	SSL (cm.g^{-1})	45.06 ± 14.62	47.84 ± 6.17	**0.0274***

Table 1: Mean alterations in growth and development parameters between WT and the PP line. The significant differences between the two genotypes are supported by a non-parametric Kruskal-Wallis test. Significant differences are indicated in bold with an asterisk. Measurements were taken at a vegetative growth stage (28 days after sowing; D28) and compared for development with measurements at an early growth stage (13 days after sowing; D13). Dry biomass allocation patterns are defined by the percentage of mean dry biomass in each compartment. Abbreviations: SLA (Specific Leaf Area); SRL (Specific Root Length); SSL (Specific Shoot Length). WT (n=23), PP (n=19).

To better understand the cause of the loss in biomass in the PP line, we analyzed carbon (%C) and nitrogen (%N) accumulation across the different tissues (**Table 2**). Results showed that nitrogen content was significantly higher in the PP line compared to the WT, particularly in the shoots (+53%). Focusing on ion uptakes in leaves and roots (**Table S4**), we identified a significant increase of nitrate ions in roots (3.3×). Conversely, carbon content was slightly lower in the PP line, most notably in the stems (-13%). As a result, the carbon-to-nitrogen ratio (C/N) was significantly decreased in the PP line, especially in the shoots.

	Carbone (%)			Nitrogen (%)			C/N ratio		
	WT mean (mean ± STDEV)	PP mean (mean ± STDEV)	p-value	WT mean (mean ± STDEV)	PP mean (mean ± STDEV)	p-value	WT mean (mean ± STDEV)	PP mean (mean ± STDEV)	p-value
Foliar blades	39.01 ± 0.41	38.66 ± 1.02	0.1616	1.72 ± 0.3	2.63 ± 0.33	**0.0005***	22.47 ± 3.96	14.82 ± 1.59	**0.0002***
Petioles	34.57 ± 0.62	33.89 ± 0.66	**0.0484***	1.34 ± 0.22	1.96 ± 0.3	**0.0005***	25.46 ± 3.91	17.57 ± 2.49	**0.0002***
Stems	31.95 ± 2.9	27.78 ± 5.75	0.0542	1.01 ± 0.18	1.22 ± 0.21	**0.0301***	31.96 ± 4.74	22.85 ± 3.68	**0.0004***
Roots	40.79 ± 0.7	40.52 ± 0.63	0.885	2.02 ± 0.12	2.27 ± 0.17	**0.006***	20.33 ± 0.95	17.89 ± 1.29	**0.0004***

Table 2: Mean alterations in Carbon (C), Nitrogen (N) contents and C/N ratio between the Wild-Type (WT) and the Psoralen Pathway (PP) lines. The variables significance between the two genotypes is supported by a non-parametric Kruskal-Wallis test. Significant differences are indicated in bold with an asterisk. Measurements were taken at a vegetative growth stage (28 days after sowing). WT (n=10), PP (n=9).

503 **4. Discussion**

504 The biosynthesis of specialized metabolites necessarily triggered a physiological cost on
505 plants, either by diverting resources for their production or through the pleiotropic effects
506 of the specialized metabolites themselves (Neilson *et al.,* 2013). This study aimed to
507 better understand the impacts of constitutive expression of four genes from the linear
508 furanocoumarin biosynthesis pathway on tomato plant physiology and growth.

509

510 **4.1. Furanocoumarins might be toxic for tomato plants**

511 Genetic modification of tomato with our construct aimed at producing psoralen
512 surprisingly resulted in a low transformation success rate (0.33%), especially when
513 compared to longer pathways already inserted with success in tomato using the same
514 GoldenBraid system with TUs also under the *CaMV*35S promoter (H. Kim *et al.,* 2025;
515 Sonawane *et al.,* 2017). Furthermore, psoralen was found only as trace amounts despite
516 that all PP transgenes were constitutively expressed (**Fig. S1c**; **Table S2g**). In parallel,
517 transcriptomic data showed significantly over-expressed genes falling in the GO
518 categories "response to stress", "response to chemicals" and other direct or indirect
519 stress-related GO classifications in the PP line (*e.g.,* photoinhibition, stress
520 phytohormones, etc) (**Fig. 5b,c**; **Fig. 6a-c**). These findings suggest a psoralen pathway-
521 dependent phytotoxicity in tomato plants, potentially linked to the production of
522 furanocoumarins (**Fig. 3a**). During the seven last decades, incremental progress has
523 highlighted a large spectrum of furanocoumarin's toxicity on a vast range of organisms,
524 including plants, occurring through a diversity of processes (*e.g.*, photocycloaddition,
525 lipid peroxidation, cytochrome P450 inhibition) (Baskin *et al.,* 1967; Bennet & Bonner,
526 1953; Diawara *et al.,* 1993; Frank *et al.,* 1998; Greenberg *et al.,* 2001; Hale *et al.,* 2004;
527 Hassan *et al.,* 2016; Kitamura *et al.,* 2005; Meepagala *et al.,* 2021; Razavi, 2010; X.-B.
528 Wang *et al.,* 2008). We therefore hypothesize that psoralen, or core intermediates and/or
529 derivatives of its biosynthetic pathway, may be toxic, or even lethal, to tomato above a
530 certain threshold. This toxicity may have impaired the regeneration of additional
531 transgenic tomato lines. However, although our transcriptomic data clearly indicated a
532 chemically related phytotoxicity in the PP line, no clear signal allowed us to pinpoint if
533 this toxicity was related to the production of psoralen and/or any intermediates, or even

534 to the accumulation of any of the other accumulated compounds, in particular
535 coumarins. However, the fact that the PP line plants appeared healthy (**Fig. S1e**) suggests
536 that they were able to circumvent the induced phytotoxicity.
537
538 **4.2. The low accumulation of furanocoumarins may reflect metabolic competition**
539 **favouring the coumarin biosynthesis pathway**
540 Metabolic engineering approaches often fall short of expectations due to our limited
541 understanding of the self-management of specialized metabolite biosynthetic pathways
542 in plants (Lynch *et al.,* 2021). In the PP line, psoralen as well as its precursors from
543 umbelliferone could be detected in almost all the plant parts but at a level below the
544 quantification limit (**Fig. 3a**), proving that our metabolic engineering approach is working
545 but not sufficiently well to allow psoralen accumulation. Given that all genes encoding
546 the enzymes essential for psoralen accumulation were appropriately expressed and the
547 corresponding enzymes proven functional (**Fig. S1e**; **Table S2g**), we suggest a metabolic
548 competition for its precursor, *p*-coumaroyl-CoA, which may be steered instead toward
549 coumarins, which were the more enriched in the PP line. Indeed, simple coumarins like
550 umbelliferone, esculetin, and scopoletin derive from *p*-coumaroyl-, caffeoyl-, and
551 feruloyl-CoA, respectively, via 2OGD-mediated *ortho*-hydroxylation followed by a
552 cyclisation that occurs spontaneously and/or is catalyzed by a COSY (C. Y. Kim *et al.,*
553 2023; Vanholme *et al.,* 2019) (**Fig. 1**). The *ortho*-hydroxylation of *p*-coumaroyl-CoA
554 constitutes the first intended metabolic step for psoralen production in the PP line. To
555 allow umbelliferone accumulation for psoralen production, we chosen the C2'H 2OGD
556 from *Pastinaca sativa* (Apiaceae) (*Ps*Diox) which was characterized *in vitro* as being
557 specific for *p*-coumaroyl-CoA (Roselli *et al.,* 2017). The marked and significant
558 accumulation of coumarins in the PP line including the formally identified esculin and
559 scopoletin (**Fig. 3**, **Fig. S3**), suggests that, *in vivo*, *Ps*Diox could share the same catalytic
560 properties as its orthologs from *Ruta graveolens* (Rutaceae), *A. thaliana* and *Ipomea*
561 *batatas* (Convolvulaceae) that also accept caffeoyl-CoA and feruloyl-CoA as substrates
562 (Matsumoto *et al.,* 2012; Vialart *et al.,* 2012; Yang *et al.,* 2015). This hypothesis is
563 supported by the accumulation of scopoletin and esculetin in plants overexpressing F6'H
564 (Beesley *et al.,* 2023; N. Wang *et al.,* 2025).

565 Non-exclusive hypotheses for the limited accumulation of psoralen may also involve
566 active regulation of competing metabolic pathways that bypass the psoralen branch (**Fig.**
567 **3**). Indeed, comparative metabolomics analysis highlighted the accumulation of
568 phenolamides (*i.e.,* fused hydroxycinnamates and amines), a natural defence compound
569 family in tomato plants (Roumani et al., 2022), in addition to coumarins (**Fig. 2**, **Table S1**).
570 In parallel, comparative transcriptomics pointed to the overexpression in the PP line of
571 genes of the core phenylpropanoid pathway putatively involved in the coumarin and
572 phenolamide biosynthesis pathways (*e.g.*, BAHD acyltransferases, Tyramine N-feruloyl
573 transferase) (**Table S2c**). Such metabolic competition for a common substrate such as
574 *p*-coumaroyl-CoA could also be further established by other factors like metabolic
575 channeling as now established in several species (Dahmani *et al.,* 2023; Lallemand *et al.,*
576 2013; Laursen *et al.,* 2016). Heterologous enzymes from different plant species may be
577 less competitive than endogenous ones in establishing metabolic channeling of
578 intermediates and co-substrates, ultimately at the expense of psoralen accumulation.
579

580 **4.3. Coumarin accumulation might underly the PP line's altered physiology**
581 **and growth**

582 The metabolomics analyses highlighted 82 metabolic features almost exclusively over-
583 accumulated in the transgenic line. Annotation outlined that primarily 4 metabolic
584 families (fatty acids, phenolamides, coumarins and furanocoumarins) were involved.
585 Among them, coumarin accumulation stood out from the other families for at least one
586 of the following reasons: (i) the accumulation of all individual coumarins followed a
587 presence/absence pattern in the PP/WT comparison (**Fig. 3a**; **Table S1**), (ii) the
588 accumulation of coumarin metabolites was detected in the three tissues (leaf, stem,
589 roots) in accordance to the constitutive expression of the PP transgenes (**Fig. 3a**) and (iii)
590 based on the targeted analyses the accumulation of coumarins reached several µg/g of
591 DW (*i.e.,* scopoletin) whereas the furanocoumarin accumulation did not reach the
592 quantification limit (**Fig. 3**). These observations made us consider that coumarins
593 accumulation may be the main stimulus of the transcriptomic, physiological and
594 developmental characteristics of the PP line. This would be consistent with previous
595 studies in which coumarins (*i.e.,* umbelliferone, scopoletin, coumarin, and daphnoretin)

596 were applied to *A. thaliana* and *Lactuca sativa* (Asteraceae), resulting in allelopathic
597 effects such as membrane peroxidation, Reactive Oxygen Species (ROS) production,
598 mitotic disruption, and photoinhibition (Araniti *et al.,* 2017; Graña *et al.,* 2017; Z. Yan *et*
599 *al.,* 2016). Our transcriptomics analysis highlighted the upregulation, in the PP line in
600 comparison to WT, of a majority of genes associated with responses to stress, chemicals,
601 organic substances and wounding (**Fig. 5b**; **Fig. 6a-c**). These categories comprise genes
602 involved in ROS detoxification (*e.g.,* glutathione-S-transferases, cytochrome P450s,
603 peroxidases, detoxification proteins, chaperones, and heat-shock proteins) (**Table S2**).
604 On the contrary, the main categories of downregulated genes in the leaves of the PP line
605 compared to WT were associated to chlorophyll biosynthesis (**Fig. 5c**; **Fig. 6d**). These
606 transcriptomics patterns suggest an active regulation of the plant oxidative status,
607 potentially mediated by an increase in the ROS detoxication processes and a decrease in
608 the ROS production linked to photosynthesis. This suggestion is supported by the healthy
609 appearance of the PP line despite the activation of all these stress signaling pathways
610 (**Fig. S1e**). As now well established, photoinhibition generally acts as a protective
611 mechanism to limit photoinduced ROS accumulation, as reviewed by Didaran *et al.,*
612 2024. In parallel, the lipid over-accumulation observed in the leaves of the PP line (**Table**
613 **1**), together with the over-expression of genes associated with lipid metabolism (*e.g.,*
614 phospholipases, aldehyde dehydrogenases, lipid biosynthesis) and membrane repair
615 (*e.g.,* lipid desaturases, acyltransferases) (**Fig. 6a**; **Table S2**), further supports the
616 occurrence of membrane damage. This lipid stress may result from coumarin-induced
617 destabilization of chloroplast integrity and photochemistry, as previously observed in *A.*
618 *thaliana* (Araniti *et al.,* 2017).
619 To further understand the impact of coumarins on tomato physiology in the PP line, we
620 investigated its effects on growth, development and resource allocation compared to the
621 WT line. First, we observed no developmental alterations in the PP line, in contrast to the
622 pronounced growth impairments reported in various plant species metabolically
623 engineered to over-accumulate scopoletin (Beesley *et al.,* 2023; Hoengenaert *et al.,*
624 2022; N. Wang *et al.,* 2025). However, F6'H knock-down lines of *Manihot esculenta*
625 (Euphorbiaceae) with reduced scopoletin accumulation have revealed key roles for this
626 compound in cassava development (*e.g.*, auxiliary budding, leaf appearance, apical

627 dominance) (Mukami *et al.,* 2024). All these elements suggests that the physiological
628 effects of coumarins on development may depend on their constitutive accumulation
629 levels and may be species-specific. This also underscores how poorly understood the
630 physiological regulation of coumarins remains, despite their strong potential to act in a
631 phytohormone-like manner, as hypothesized for an auxin-like effect of scopoletin by
632 Graña *et al.,* 2017.
633 Morphological analysis of the PP line revealed a significant biomass reduction,
634 particularly of the leaves (**Table 1**). A similar biomass loss was previously reported in *A.*
635 *thaliana* supplemented with coumarin or scopoletin (Araniti *et al.,* 2017; Graña *et al.,*
636 2017) and was partly attributed to photoinhibition observed in the leaves, similarly to
637 what we found in the PP line according to transcriptomic data (**Fig. 6d**). In addition, we
638 also observed a downregulation of a few genes putatively involved in sugar storage (*i.e.,*
639 starch synthase) and numerous genes putatively involved in sugar metabolism and cell
640 wall remobilization (**Table S2c,d**). Their differential expression may help explain the
641 biomass loss observed, which cannot be exclusively attributed to carbon content
642 reduction, as this decrease is substantially lower than the 21% drop in biomass (**Tables**
643 **2 and 3**). Considering that most of the biomass components were measured (*e.g.,*
644 carbon, nitrogen, ions) (**Table 2**; **Table S4**), we suggest a concomitant reduction in
645 oxygen-rich compounds such as sugars. In parallel, significant increase of specific leave
646 surface (SLA; +39%) underlies a biomass loss that is distributed within thinner leaves
647 (**Table 1**). Taken together, these elements suggest that coumarins may trigger a 'slimming
648 effect', leading to biomass reduction, primarily in tomato leaves, as a potential response
649 to coumarin-induced phytotoxicity.
650 Thioacidolysis revealed that scopoletin was incorporated into the cell wall (**Fig. 4c**),
651 albeit at a level approximately 10 to 100 times lower than found in *A. thaliana* and *Glycine*
652 *max* (Fabaceae) (Beesley *et al.,* 2023; Hoengenaert *et al.,* 2022). Although only trace
653 amounts of scopoletin accumulated in the cell wall, which prevented validation of its
654 integration into the lignin polymer by NMR, it is reasonable to consider that a small
655 fraction of scopoletin could be incorporated into the lignin polymer. Although the stem
656 cell wall appears to be a key storage compartment for coumarins (Beesley *et al.,* 2023),
657 glycosylated coumarins are stored in vacuoles, *e.g.,* in *A. thaliana* roots (Robe *et al.,*

658 2021). Both vacuolar storage and cell wall transfer are well established toxicity mitigation
659 processes (Weng *et al.,* 2021). Our metabolic and phenotypic data suggest that even a
660 modest accumulation of scopoletin (~1-5 µg/g DW), has to be mitigated in the PP line.
661 Finally, we found that the significant increase in nitrogen content in the upper parts of the
662 PP line coincided with enhanced nitrate uptake by the roots. Catecholic coumarins such
663 as esculetin and fraxetin are well-known to facilitate iron uptake from the soil in plants
664 (H. H. Tsai & Schmidt, 2017). Our data suggest that coumarins accumulation, primarily
665 esculetin, is concomitant with nitrate uptake, highlighting a potential role of coumarins
666 in this process. A similar contribution of coumarins already reported in *Triticum durum*
667 and *Zea mays* (both Poaceae) (Abenavoli *et al.,* 2001; Lupini *et al.,* 2018).
668

669 **5. Conclusion**

670 The production of psoralen in tomato proved to be more challenging than the mere
671 expression of the biosynthetic genes as it potentially led to pronounced phytotoxicity. Our
672 results suggests that the accumulation of coumarins at concentrations of 1-5 µg/g of DW
673 in tomato plants could induces several levels of regulation: (i) xenobiotic stress leading
674 to oxidative stress, which the plant can adapt; (ii) a photoinhibition and an increase in
675 metabolism inducing a biomass slimming possibly in response to oxidative stress; and
676 (iii) a modification of the nitrogen and nitrate levels. Our results indicate that, although
677 coumarins hold substantial agronomic potential (non-toxic to pollinators, facilitating iron
678 uptake, shaping root microbiota, etc) (Cosme et al., 2021; H.-H. Tsai et al., 2018; Zhou et
679 al., 2023), their role in plant defense entails a growth cost even at low content. A
680 counterpart that should be carefully considered and ideally mitigated, following a more
681 precise delineation of the regulatory pathways of coumarins underlying the identified
682 physiological impacts, before pursuing potential viable applications.
683

684 **6. Acknowledgments**

685 We would like to thank Alexandre Olry, Claude Gallois and David Marcolet members of
686 the Experimental phytotronic platform of Lorraine PEPLor (Université de Lorraine, France)
687 for their technical assistance, Cédric Paris from the Metabolomic and Structural Analytic
688 Platform facility (PASM, Université de Lorraine, France) as well as Geert Goeminne and

Sandrien Desmet from the Metabolomic Core (VIB, Gent, Belgium). We thank Sarah Liu for her assistance on NMR sample preparation. We thank Florent Magot (BBV, Université de Tours) and Florent Ducrocq for assistance in the critical analysis of the metabolomic data as well as Eugène Maurey for the critical statistical analysis of morphophysiological data.

7. Competing interests

None declared

8. Author contributions

GG, CV and AB, designed and assembled the PP genetic construction. AB, MR, CV, AF and GG participated to transgenic lines regeneration. AB, AF and MR cultivated and harvested the tomato plants. AB, FH and RL generated and analyzed the transcriptomic data. AB, JG and RL generated and analyzed the metabolomic data. AB, LH, JR and WB analyzed the lignin composition. AB, CR and RL generated and analyzed the morphophysiological data. AB, RL and AH conceptualized the project and wrote the article. WB, AH and RL supervised the project. All co-authors reviewed the article.

9. Funding sources

AB was financially supported by a PhD grant provided by the French Government and Grand Est Region. AB benefited from the mobility programs DREAM provided by 'Lorraine Université d'Excellence', funded by the ANR 'Investissements d'avenir' (grant no. 15-004) and from the DESSE facility funded by the INRAE. WB was funded by the interuniversity Bijzonder Onderzoeksfonds (iBOF) NextBioRef. JR was supported by the Great Lakes Bioenergy Research Center, U.S. Department of Energy, Office of Science, Biological and Environmental Research Program, under Award Number DE-SC0018409.

10. Bibliography

Abenavoli, M. R., De Santis, C., Sidari, M., Sorgonà, A., Badiani, M., & Cacco, G. (2001). Influence of coumarin on the net nitrate uptake in durum wheat. New Phytologist, 150(3), 619-627. https://doi.org/10.1046/j.1469-8137.2001.00119.x

Alves-Carvalho, S., Gazengel, K., Bretaudeau, A., Robin, S., Daval, S., & Legeai, F. (2021). AskoR, A R Package for Easy RNASeq Data Analysis. Proceedings of The 1st

International Electronic Conference on Entomology, 10646. https://doi.org/10.3390/IECE-10646

Araniti, F., Scognamiglio, M., Chambery, A., Russo, R., Esposito, A., D'Abrosca, B., Fiorentino, A., Lupini, A., Sunseri, F., & Abenavoli, M. R. (2017). Highlighting the effects of coumarin on adult plants of *Arabidopsis thaliana* (L.) Heynh. By an integrated -omic approach. Journal of Plant Physiology, 213, 30-41. https://doi.org/10.1016/j.jplph.2017.02.013

Baskin, J. M., Ludlow, C. J., Harris, T. M., & Wolf, F. T. (1967). Psoralen, an inhibitor in the seeds of *Psoralea subacaulis* (Leguminosae). Phytochemistry, 6(9), 1209-1213. https://doi.org/10.1016/S0031-9422(00)86083-5

Beesley, A., Beyer, S. F., Wanders, V., Levecque, S., Bredenbruch, S., Habash, S. S., Schleker, A. S. S., Gätgens, J., Oldiges, M., Schultheiss, H., Conrath, U., & Langenbach, C. J. G. (2023). Engineered coumarin accumulation reduces mycotoxin-induced oxidative stress and disease susceptibility. Plant Biotechnology Journal, 21(12), 2490-2506. https://doi.org/10.1111/pbi.14144

Bennet, & Bonner. (1953). Isolation of Plant Growth Inhibitors from *Thamnosma montana*. 6. American Journal of Botany, 29-33. https://doi.org/10.2307/2438489

Bolger, A. M., Lohse, M., & Usadel, B. (2014). Trimmomatic : A flexible trimmer for Illumina sequence data. Bioinformatics, 30(15), 2114-2120. https://doi.org/10.1093/bioinformatics/btu170

Bouillé, A., Larbat, R., Kumari, R., Olry, A., Charles, C., Nelson, D. R., Thornton, J., Villard, C., & Hehn, A. (2025). Lineage-specific patterns in the Moraceae family allow identification of convergent P450 enzymes involved in furanocoumarin biosynthesis. New Phytologist. https://doi.org/10.1111/nph.20381

Chassagne, F., Cabanac, G., Hubert, G., David, B., & Marti, G. (2019). The landscape of natural product diversity and their pharmacological relevance from a focus on the Dictionary of Natural Products®. Phytochemistry Reviews, 18(3), 601-622. https://doi.org/10.1007/s11101-019-09606-2

Cosme, M., Fernández, I., Declerck, S., van der Heijden, M. G. A., & Pieterse, C. M. J. (2021). A coumarin exudation pathway mitigates arbuscular mycorrhizal incompatibility in *Arabidopsis thaliana*. Plant Molecular Biology, 106(4-5), 319-334. https://doi.org/10.1007/s11103-021-01143-x

Dahmani, I., Qin, K., Zhang, Y., & Fernie, A. R. (2023). The formation and function of plant metabolons. The Plant Journal, 114(5), 1080-1092. https://doi.org/10.1111/tpj.16179

Diawara, M. M., Trumble, J. T., White, K. K., Carson, W. G., & Martinez, L. A. (1993). Toxicity of linear furanocoumarins to *Spodoptera exigua*: Evidence for antagonistic interactions. Journal of Chemical Ecology, 19(11), 2473-2484. https://doi.org/10.1007/BF00980684

Didaran, F., Kordrostami, M., Ghasemi-Soloklui, A. A., Pashkovskiy, P., Kreslavski, V., Kuznetsov, V., & Allakhverdiev, S. I. (2024). The mechanisms of photoinhibition and repair in plants under high light conditions and interplay with abiotic stressors. Journal of Photochemistry and Photobiology B: Biology, 259, 113004. https://doi.org/10.1016/j.jphotobiol.2024.113004

Djoumbou Feunang, Y., Eisner, R., Knox, C., Chepelev, L., Hastings, J., Owen, G., Fahy, E., Steinbeck, C., Subramanian, S., Bolton, E., Greiner, R., & Wishart, D. S. (2016). ClassyFire : Automated chemical classification with a comprehensive, computable

taxonomy. Journal of Cheminformatics, 8(1), 61. https://doi.org/10.1186/s13321-016-0174-y

Dührkop, K., Fleischauer, M., Ludwig, M., Aksenov, A. A., Melnik, A. V., Meusel, M., Dorrestein, P. C., Rousu, J., & Böcker, S. (2019). SIRIUS 4 : A rapid tool for turning tandem mass spectra into metabolite structure information. Nature Methods, 16(4), 299-302. https://doi.org/10.1038/s41592-019-0344-8

Frank, S., Caffieri, S., Raffaelli, A., Vedaldi, D., & Dall'Acqua, F. (1998). Characterization of psoralen-oleic acid cycloadducts and their possible involvement in membrane photodamage. Journal of Photochemistry and Photobiology B: Biology, 44(1), 39-44. https://doi.org/10.1016/S1011-1344(98)00103-1

Ge, S. X., Jung, D., & Yao, R. (2020). ShinyGO : A graphical gene-set enrichment tool for animals and plants. Bioinformatics, 36(8), 2628-2629. https://doi.org/10.1093/bioinformatics/btz931

Godichon-Baggioni, A., Maugis-Rabusseau, C., & Rau, A. (2019). Clustering transformed compositional data using K -means, with applications in gene expression and bicycle sharing system data. Journal of Applied Statistics, 46(1), 47-65. https://doi.org/10.1080/02664763.2018.1454894

Graña, E., Costas-Gil, A., Longueira, S., Celeiro, M., Teijeira, M., Reigosa, M. J., & Sánchez-Moreiras, A. M. (2017a). Auxin-like effects of the natural coumarin scopoletin on A*rabidopsis* cell structure and morphology. Journal of Plant Physiology, 218, 45-55. https://doi.org/10.1016/j.jplph.2017.07.007

Graña, E., Costas-Gil, A., Longueira, S., Celeiro, M., Teijeira, M., Reigosa, M. J., & Sánchez-Moreiras, A. M. (2017b). Auxin-like effects of the natural coumarin scopoletin on Arabidopsis cell structure and morphology. Journal of Plant Physiology, 218, 45-55. https://doi.org/10.1016/j.jplph.2017.07.007

Greenberg, R. B., Alberti, M., Hearst, J. E., Chua, M. A., & Saffran, W. A. (2001). Recombinational and Mutagenic Repair of Psoralen Interstrand Cross-links in *Saccharomyces cerevisiae*. Journal of Biological Chemistry, 276(34), 31551-31560. https://doi.org/10.1074/jbc.M103588200

Hale, A. L., Meepagala, K. M., Oliva, A., Aliotta, G., & Duke, S. O. (2004). Phytotoxins from the Leaves of *Ruta graveolens*. Journal of Agricultural and Food Chemistry, 52(11), 3345-3349. https://doi.org/10.1021/jf0497298

Han, L., Zhang, L., He, Y., Liao, L., Li, J., Xu, S., Zhao, Y., Bian, X., & Xia, Y. (2023). Three carbon-/oxygen-prenyltransferases responsible for furanocoumarin synthesis in *Angelica dahurica*. Industrial Crops and Products, 200, 116814. https://doi.org/10.1016/j.indcrop.2023.116814

Hassan, Mohd. Z., Osman, H., Ali, M. A., & Ahsan, M. J. (2016). Therapeutic potential of coumarins as antiviral agents. European Journal of Medicinal Chemistry, 123, 236-255. https://doi.org/10.1016/j.ejmech.2016.07.056

He, Z., Webster, S., & He, S. Y. (2022). Growth–defense trade-offs in plants. Current Biology, 32(12), R634-R639. https://doi.org/10.1016/j.cub.2022.04.070

Hehmann, M., Lukačin, R., Ekiert, H., & Matern, U. (2004). Furanocoumarin biosynthesis in *Ammi majus L.* : Cloning of bergaptol O-methyltransferase. European Journal of Biochemistry, 271(5), 932-940. https://doi.org/10.1111/j.1432-1033.2004.03995.x

Hellens, R. P., Edwards, E. A., Leyland, N. R., Bean, S., & Mullineaux, P. M. (2000). pGreen : A versatile and flexible binary Ti vector for *Agrobacterium*-mediated plant

transformation. Plant Molecular Biology, 42(6), 819-832. https://doi.org/10.1023/A:1006496308160

Hoengenaert, L., Wouters, M., Kim, H., De Meester, B., Morreel, K., Vandersyppe, S., Pollier, J., Desmet, S., Goeminne, G., Ralph, J., Boerjan, W., & Vanholme, R. (2022). Overexpression of the scopoletin biosynthetic pathway enhances lignocellulosic biomass processing. Science Advances, 8(28), eabo5738. https://doi.org/10.1126/sciadv.abo5738

Hoffmann, M. A., Nothias, L.-F., Ludwig, M., Fleischauer, M., Gentry, E. C., Witting, M., Dorrestein, P. C., Dührkop, K., & Böcker, S. (2021). Assigning confidence to structural annotations from mass spectra with COSMIC. Bioinformatics. https://doi.org/10.1101/2021.03.18.435634

Ji, J., Han, X., Zang, L., Li, Y., Lin, L., Hu, D., Sun, S., Ren, Y., Maker, G., Lu, Z., & Wang, L. (2024). Integrative multi-omics data elucidating the biosynthesis and regulatory mechanisms of furanocoumarins in *Angelica dahurica*. https://doi.org/10.1101/2024.07.23.604792

Jian, X., Zhao, Y., Wang, Z., Li, S., Li, L., Luo, J., & Kong, L. (2020). Two CYP71AJ enzymes function as psoralen synthase and angelicin synthase in the biosynthesis of furanocoumarins in *Peucedanum praeruptorum Dunn*. Plant Molecular Biology, 104(3), 327-337. https://doi.org/10.1007/s11103-020-01045-4

Karamat, F., Olry, A., Munakata, R., Koeduka, T., Sugiyama, A., Paris, C., Hehn, A., Bourgaud, F., & Yazaki, K. (2014). A coumarin-specific prenyltransferase catalyzes the crucial biosynthetic reaction for furanocoumarin formation in parsley. The Plant Journal, 77(4), 627-638. https://doi.org/10.1111/tpj.12409

Kim, C. Y., Mitchell, A. J., Kastner, D. W., Albright, C. E., Gutierrez, M. A., Glinkerman, C. M., Kulik, H. J., & Weng, J.-K. (2023). Emergence of a proton exchange-based isomerization and lactonization mechanism in the plant coumarin synthase COSY. Nature Communications, 14(1), 597. https://doi.org/10.1038/s41467-023-36299-1

Kim, H., Liu, L., Han, L., Park, K., Kim, H. J., Nguyen, T., Nazarenus, T. J., Cahoon, R. E., Haslam, R. P., Ciftci, O., Napier, J. A., & Cahoon, E. B. (2025). Oilseed-based metabolic engineering of astaxanthin and related ketocarotenoids using a plant-derived pathway : Lab-to-field-to-application. Plant Biotechnology Journal, pbi.70148. https://doi.org/10.1111/pbi.70148

Kim, H. W., Wang, M., Leber, C. A., Nothias, L.-F., Reher, R., Kang, K. B., Van Der Hooft, J. J. J., Dorrestein, P. C., Gerwick, W. H., & Cottrell, G. W. (2021). NPClassifier : A Deep Neural Network-Based Structural Classification Tool for Natural Products. Journal of Natural Products, 84(11), 2795-2807. https://doi.org/10.1021/acs.jnatprod.1c00399

Kitamura, N., Kohtani, S., & Nakagaki, R. (2005). Molecular aspects of furocoumarin reactions : Photophysics, photochemistry, photobiology, and structural analysis. Journal of Photochemistry and Photobiology C: Photochemistry Reviews, 6(2-3), 168-185. https://doi.org/10.1016/j.jphotochemrev.2005.08.002

Krieger, C., Roselli, S., Kellner-Thielmann, S., Galati, G., Schneider, B., Grosjean, J., Olry, A., Ritchie, D., Matern, U., Bourgaud, F., & Hehn, A. (2018). The CYP71AZ P450 Subfamily : A Driving Factor for the Diversification of Coumarin Biosynthesis in Apiaceous Plants. Frontiers in Plant Science, 9, 820. https://doi.org/10.3389/fpls.2018.00820

Lallemand, B., Erhardt, M., Heitz, T., & Legrand, M. (2013). Sporopollenin Biosynthetic Enzymes Interact and Constitute a Metabolon Localized to the Endoplasmic Reticulum of Tapetum Cells. Plant Physiology, 162(2), 616-625. https://doi.org/10.1104/pp.112.213124

Larbat, R., Hehn, A., Hans, J., Schneider, S., Jugdé, H., Schneider, B., Matern, U., & Bourgaud, F. (2009). Isolation and Functional Characterization of CYP71AJ4 Encoding for the First P450 Monooxygenase of Angular Furanocoumarin Biosynthesis. Journal of Biological Chemistry, 284(8), 4776-4785. https://doi.org/10.1074/jbc.M807351200

Larbat, R., Kellner, S., Specker, S., Hehn, A., Gontier, E., Hans, J., Bourgaud, F., & Matern, U. (2007). Molecular Cloning and Functional Characterization of Psoralen Synthase, the First Committed Monooxygenase of Furanocoumarin Biosynthesis. Journal of Biological Chemistry, 282(1), 542-554. https://doi.org/10.1074/jbc.M604762200

Laursen, T., Borch, J., Knudsen, C., Bavishi, K., Torta, F., Martens, H. J., Silvestro, D., Hatzakis, N. S., Wenk, M. R., Dafforn, T. R., Olsen, C. E., Motawia, M. S., Hamberger, B., Møller, B. L., & Bassard, J.-E. (2016). Characterization of a dynamic metabolon producing the defense compound dhurrin in sorghum. Science, 354(6314), 890-893. https://doi.org/10.1126/science.aag2347

Li, H., & Durbin, R. (2009). Fast and accurate short read alignment with Burrows–Wheeler transform. Bioinformatics, 25(14), 1754-1760. https://doi.org/10.1093/bioinformatics/btp324

Liao, Y., Smyth, G. K., & Shi, W. (2014). featureCounts : An efficient general purpose program for assigning sequence reads to genomic features. Bioinformatics, 30(7), 923-930. https://doi.org/10.1093/bioinformatics/btt656

Lu, F., Wang, C., Chen, M., Yue, F., & Ralph, J. (2021). A facile spectroscopic method for measuring lignin content in lignocellulosic biomass. Green Chemistry, 23(14), 5106-5112. https://doi.org/10.1039/D1GC01507A

Ludwig, M., Nothias, L.-F., Dührkop, K., Koester, I., Fleischauer, M., Hoffmann, M. A., Petras, D., Vargas, F., Morsy, M., Aluwihare, L., Dorrestein, P. C., & Böcker, S. (2019). ZODIAC : Database-independent molecular formula annotation using Gibbs sampling reveals unknown small molecules. Bioinformatics. https://doi.org/10.1101/842740

Lupini, A., Araniti, F., Mauceri, A., Princi, M. P., Sorgonà, A., Sunseri, F., Varanini, Z., & Abenavoli, M. R. (2018). Coumarin enhances nitrate uptake in maize roots through modulation of plasma membrane H+ - ATP ase activity. Plant Biology, 20(2), 390-398. https://doi.org/10.1111/plb.12674

Lynch, J. H., Huang, X.-Q., & Dudareva, N. (2021). Silent constraints : The hidden challenges faced in plant metabolic engineering. Current Opinion in Biotechnology, 69, 112-117. https://doi.org/10.1016/j.copbio.2020.12.014

Maeda, H. A., & Fernie, A. R. (2021). Evolutionary History of Plant Metabolism. Annual Review of Plant Biology, 72(1), 185-216. https://doi.org/10.1146/annurev-arplant-080620-031054

Matsumoto, S., Mizutani, M., Sakata, K., & Shimizu, B.-I. (2012). Molecular cloning and functional analysis of the ortho-hydroxylases of p-coumaroyl coenzyme A/feruloyl coenzyme A involved in formation of umbelliferone and scopoletin in sweet potato, Ipomoea batatas (L.) Lam. Phytochemistry, 74, 49-57. https://doi.org/10.1016/j.phytochem.2011.11.009

Meepagala, K. M., Bracken, A. K., Fronczek, F. R., Johnson, R. D., Wedge, D. E., & Duke, S. O. (2021). Furanocoumarin with Phytotoxic Activity from the Leaves of *Amyris elemifera* (Rutaceae). ACS Omega, 6(1), 401-407. https://doi.org/10.1021/acsomega.0c04778

Morris, J. L., Puttick, M. N., Clark, J. W., Edwards, D., Kenrick, P., Pressel, S., Wellman, C. H., Yang, Z., Schneider, H., & Donoghue, P. C. J. (2018). The timescale of early land plant evolution. Proceedings of the National Academy of Sciences, 115(10). https://doi.org/10.1073/pnas.1719588115

Mukami, A., Juma, B. S., Mweu, C., Oduor, R., & Mbinda, W. (2024). CRISPR-Cas9-induced targeted mutagenesis of feruloyl CoA 6'-hydroxylase gene reduces postharvest physiological deterioration in cassava roots. Postharvest Biology and Technology, 208, 112649. https://doi.org/10.1016/j.postharvbio.2023.112649

Munakata, R., Olry, A., Karamat, F., Courdavault, V., Sugiyama, A., Date, Y., Krieger, C., Silie, P., Foureau, E., Papon, N., Grosjean, J., Yazaki, K., Bourgaud, F., & Hehn, A. (2016). Molecular evolution of parsnip (*Pastinaca sativa*) membrane-bound prenyltransferases for linear and/or angular furanocoumarin biosynthesis. New Phytologist, 211(1), 332-344. https://doi.org/10.1111/nph.13899

Neal, J. J., & Wu, D. (1994). Inhibition of Insect Cytochromes P450 by Furanocoumarins. Pesticide Biochemistry and Physiology, 50(1), 43-50. https://doi.org/10.1006/pest.1994.1056

Neilson, E. H., Goodger, J. Q. D., Woodrow, I. E., & Møller, B. L. (2013). Plant chemical defense : At what cost? Trends in Plant Science, 18(5), 250-258. https://doi.org/10.1016/j.tplants.2013.01.001

Razavi, S. M. (2010). Plant Coumarins as Allelopathic Agents. International Journal of Biological Chemistry, 5(1), 86-90. https://doi.org/10.3923/ijbc.2011.86.90

Robe, K., Conejero, G., Gao, F., Lefebvre-Legendre, L., Sylvestre-Gonon, E., Rofidal, V., Hem, S., Rouhier, N., Barberon, M., Hecker, A., Gaymard, F., Izquierdo, E., & Dubos, C. (2021). Coumarin accumulation and trafficking in *Arabidopsis thaliana*: A complex and dynamic process. New Phytologist, 229(4), 2062-2079. https://doi.org/10.1111/nph.17090

Robinson, M. D., McCarthy, D. J., & Smyth, G. K. (2010). edgeR : A Bioconductor package for differential expression analysis of digital gene expression data. Bioinformatics, 26(1), 139-140. https://doi.org/10.1093/bioinformatics/btp616

Rolando, C., Monties, B., & Lapierre, C. (1992). Thioacidolysis. In S. Y. Lin & C. W. Dence (Éds.), Methods in Lignin Chemistry (p. 334-349). Springer Berlin Heidelberg. https://doi.org/10.1007/978-3-642-74065-7_23

Roselli, S., Olry, A., Vautrin, S., Coriton, O., Ritchie, D., Galati, G., Navrot, N., Krieger, C., Vialart, G., Bergès, H., Bourgaud, F., & Hehn, A. (2017). A bacterial artificial chromosome (BAC) genomic approach reveals partial clustering of the furanocoumarin pathway genes in parsnip. The Plant Journal, 89(6), 1119-1132. https://doi.org/10.1111/tpj.13450

Roumani, M., Le Bot, J., Boisbrun, M., Magot, F., Péré, A., Robin, C., Hilliou, F., & Larbat, R. (2022). Transcriptomics and metabolomics analyses reveal high induction of the phenolamide pathway in tomato plants attacked by the leafminer *Tuta absoluta*. Metabolites, 12(6), 484. https://doi.org/10.3390/metabo12060484

Sarker, S. D., & Nahar, L. (2017). Progress in the chemistry of naturally occurring coumarins. In A. D. Kinghorn, H. Falk, S. Gibbons, & J. Kobayashi (Éds.), Progress in the

Chemistry of Organic Natural Products 106 (Vol. 106, p. 241-304). Springer International Publishing. https://doi.org/10.1007/978-3-319-59542-9_3

Sarrion-Perdigones, A., Falconi, E. E., Zandalinas, S. I., Juárez, P., Fernández-del-Carmen, A., Granell, A., & Orzaez, D. (2011). GoldenBraid : An iterative cloning system for standardized assembly of reusable genetic modules. PLoS ONE, 6(7), e21622. https://doi.org/10.1371/journal.pone.0021622

Sarrion-Perdigones, A., Vazquez-Vilar, M., Palaci, J., Castelijns, B., Forment, J., Ziarsolo, P., Blanca, J., Granell, A., & Orzaez, D. (2013). GoldenBraid 2.0 : A comprehensive DNA assembly framework for plant synthetic biology. PLANT PHYSIOLOGY, 162(3), 1618-1631. https://doi.org/10.1104/pp.113.217661

Sonawane, P. D., Pollier, J., Panda, S., Szymanski, J., Massalha, H., Yona, M., Unger, T., Malitsky, S., Arendt, P., Pauwels, L., Almekias-Siegl, E., Rogachev, I., Meir, S., Cárdenas, P. D., Masri, A., Petrikov, M., Schaller, H., Schaffer, A. A., Kamble, A., ... Aharoni, A. (2017). Plant cholesterol biosynthetic pathway overlaps with phytosterol metabolism. Nature Plants, 3(1), 16205. https://doi.org/10.1038/nplants.2016.205

Tsai, H. H., & Schmidt, W. (2017). Mobilization of Iron by Plant-Borne Coumarins. Trends in Plant Science, 22(6), 538-548. https://doi.org/10.1016/j.tplants.2017.03.008

Vanholme, R., Sundin, L., Seetso, K. C., Kim, H., Liu, X., Li, J., De Meester, B., Hoengenaert, L., Goeminne, G., Morreel, K., Haustraete, J., Tsai, H.-H., Schmidt, W., Vanholme, B., Ralph, J., & Boerjan, W. (2019). COSY catalyses trans–cis isomerization and lactonization in the biosynthesis of coumarins. Nature Plants, 5(10), 1066-1075. https://doi.org/10.1038/s41477-019-0510-0

Tsai, H.-H., Rodríguez-Celma, J., Lan, P., Wu, Y.-C., Vélez-Bermúdez, I. C., & Schmidt, W. (2018). Scopoletin 8-Hydroxylase-mediated fraxetin production Is crucial for iron mobilization. Plant Physiology, 177(1), 194-207. https://doi.org/10.1104/pp.18.00178

Vialart, G., Hehn, A., Olry, A., Ito, K., Krieger, C., Larbat, R., Paris, C., Shimizu, B., Sugimoto, Y., Mizutani, M., & Bourgaud, F. (2012). A 2-oxoglutarate-dependent dioxygenase from *Ruta graveolens L*. exhibits *p*-coumaroyl CoA 2'-hydroxylase activity (C2'H) : A missing step in the synthesis of umbelliferone in plants: C2'H involved in umbelliferone synthesis. The Plant Journal, 70(3), 460-470. https://doi.org/10.1111/j.1365-313X.2011.04879.x

Villard, C., Munakata, R., Kitajima, S., Velzen, R., Schranz, M. E., Larbat, R., & Hehn, A. (2021). A new P450 involved in the furanocoumarin pathway underlies a recent case of convergent evolution. New Phytologist, 231(5), 1923-1939. https://doi.org/10.1111/nph.17458

Wang, K., Zeng, H., Dai, Y., Wang, Z., Tang, H., Li, J., Lu, X., Jiang, N., Xie, G., Zhu, Y., Zhao, Y., & Qin, M. (2024). Three types of enzymes complete the furanocoumarins core skeleton biosynthesis in *Angelica sinensis*. Phytochemistry, 222, 114102. https://doi.org/10.1016/j.phytochem.2024.114102

Wang, N., Takada, M., Sakamoto, S., Vanholme, R., Goeminne, G., Kim, H., Nagano, S., Takata, N., Kamimura, N., Uesugi, M., Izumi-Nakagawa, A., Masai, E., Mitsuda, N., Boerjan, W., Ralph, J., & Kajita, S. (2025). Effects of feruloyl-CoA 6'-hydroxylase 1 overexpression on lignin and cell wall characteristics in transgenic hybrid aspen. Frontiers in Plant Science, 16, 1543168. https://doi.org/10.3389/fpls.2025.1543168

Wang, X.-B., Li, G.-H., Li, L., Zheng, L.-J., Huang, R., & Zhang, K.-Q. (2008). Nematicidal coumarins from *Heracleum candicans Wall*. Natural Product Research, 22(8), 666-671. https://doi.org/10.1080/14786410701766463

Weng, J.-K., Lynch, J. H., Matos, J. O., & Dudareva, N. (2021). Adaptive mechanisms of plant specialized metabolism connecting chemistry to function. Nature Chemical Biology, 17(10), 1037-1045. https://doi.org/10.1038/s41589-021-00822-6

Yan, Z., Wang, D., Cui, H., Zhang, D., Sun, Y., Jin, H., Li, X., Yang, X., Guo, H., He, X., Pan, L., Ren, X., Guo, K., & Qin, B. (2016). Phytotoxicity mechanisms of two coumarin allelochemicals from *Stellera chamaejasme* in lettuce seedlings. Acta Physiologiae Plantarum, 38(10), 248. https://doi.org/10.1007/s11738-016-2270-z

Yang, S.-M., Shim, G. Y., Kim, B.-G., & Ahn, J.-H. (2015). Biological synthesis of coumarins in *Escherichia coli*. Microbial Cell Factories, 14(1), 65. https://doi.org/10.1186/s12934-015-0248-y

Zhao, Y., Wang, N., Zeng, Z., Xu, S., Huang, C., Wang, W., Liu, T., Luo, J., & Kong, L. (2016). Cloning, functional characterization, and catalytic mechanism of a bergaptol O-methyltransferase from *Peucedanum praeruptorum Dunn*. Frontiers in Plant Science, 7. https://doi.org/10.3389/fpls.2016.00722

Zhou, H., Jian, Y., Shao, Q., Guo, F., Zhang, M., Wan, F., Yang, L., Liu, Y., Yang, L., Li, Y., Yang, P., Li, Z., Li, S., & Ding, W. (2023). Development of sustainable insecticide candidates for protecting pollinators: Insight into the bioactivities, selective mechanism of action and QSAR of natural coumarin derivatives against aphids. Journal of Agricultural and Food Chemistry, 71(47), 18359-18374. https://doi.org/10.1021/acs.jafc.3c03493

11. Supplemental data

a

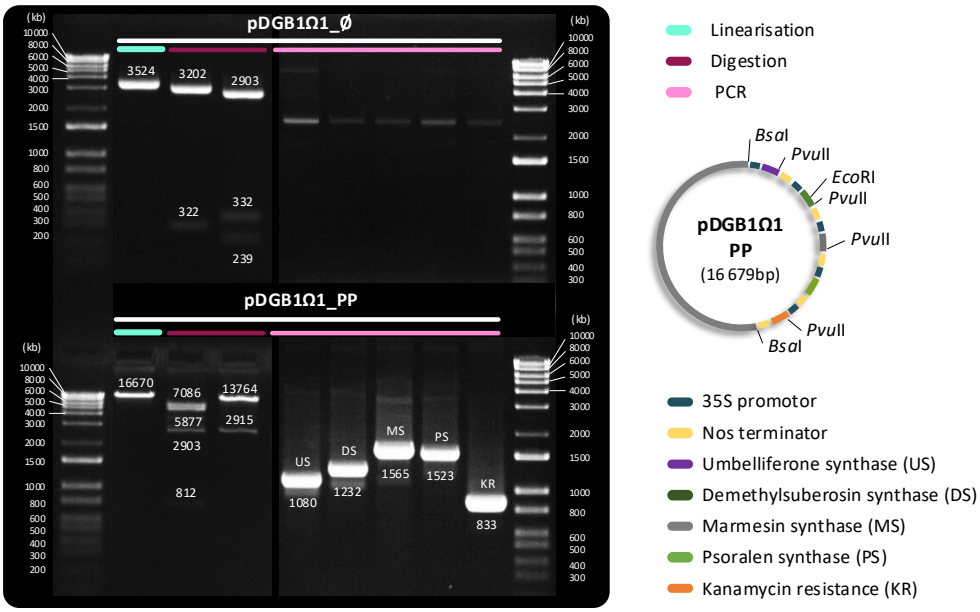

b

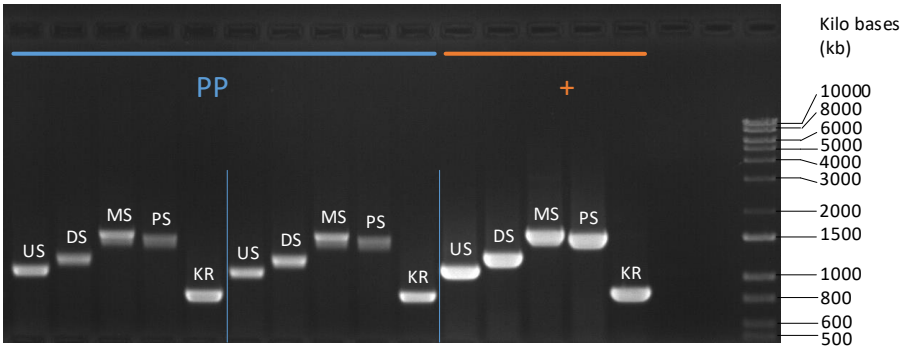

c

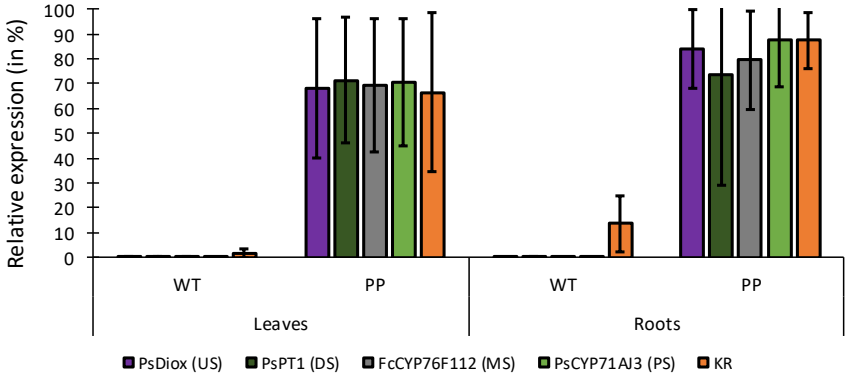

1025
1026
1027

d

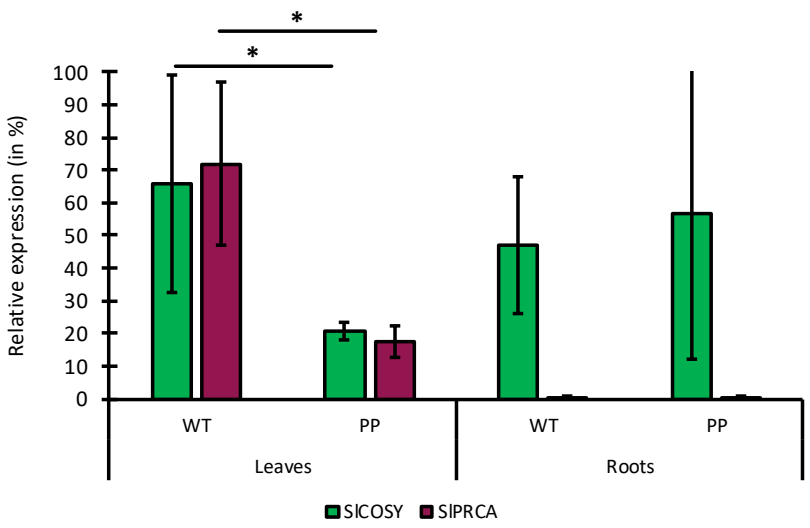

e

Wild-Type (WT) line

Psoralen Pathway (PP) line

Figure S1: Establishment of the Psoralen Pathway (PP) line. (**a**) Electrophoresis gel verification after linearization, restriction, and PCR of the pDGB1Ω1_PP construct and the empty vector pDGB1Ω1_Ø as a negative control. (**b**) Gel electrophoresis of PCR fragments verification of two T1 transformed lines using genomic DNA for the 5 genes of the PP construct. Positive control (+)

is a PCR amplification of the pDGB1Ω1_PP plasmid under the same conditions. (**c**) Expression validation of the five PP transgenes using cDNA from roots and leaves of the WT and PP lines for each conditions in triplicate. (**d**) Expression validation of two genes (*Sl*RCA: Solyc10g086580; *Sl*COSY: Solyc06g082860) significantly down- and upregulated in the PP line according to transcriptomic data, respectively. Actin and GAPDH were used as housekeeping reference genes. (**e**) Photographs of representative tomato plants (*Solanum lycopersicum* var. Wva106, Solanaceae) from the Wild-Type (left) and PP (right) lines, 28 days post-sowing under controlled, non-limiting growth conditions.

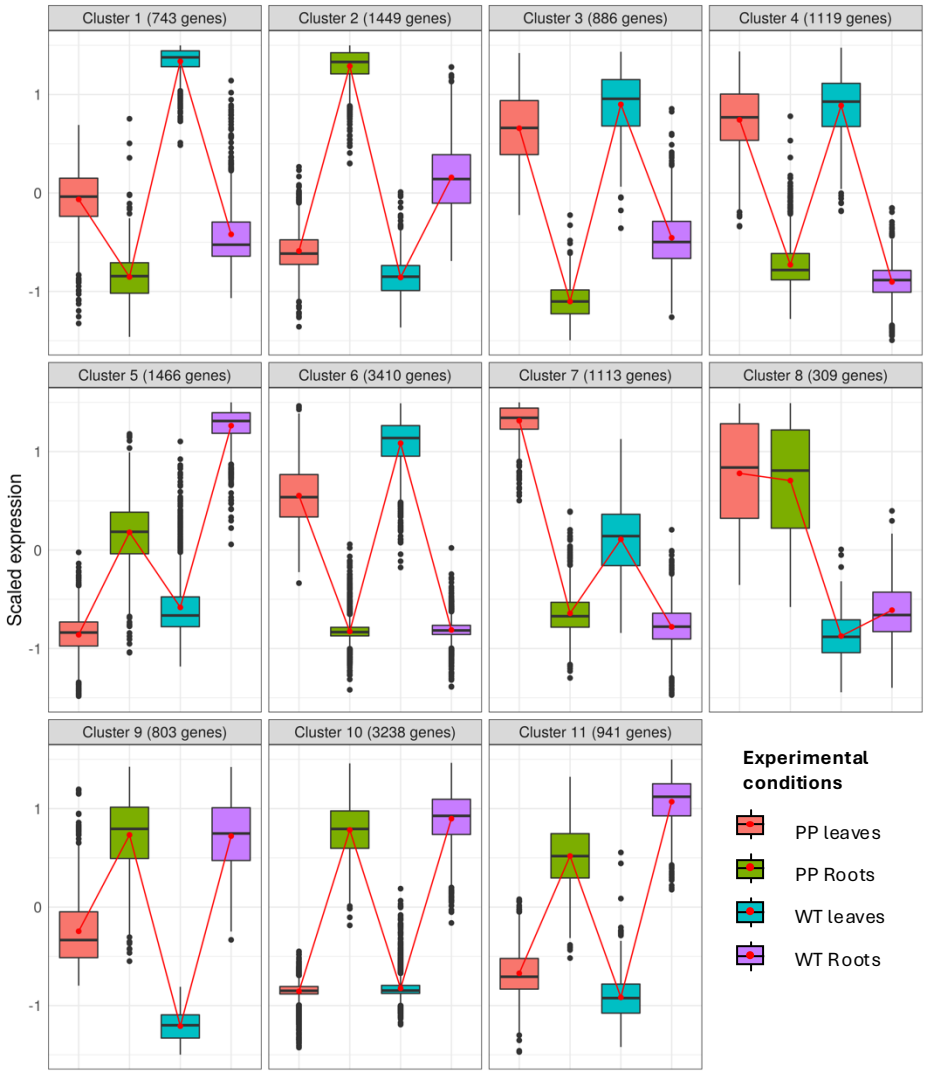

Figure S2: Clustering analysis of the specific gene regulation between the Psoralen Pathway (PP) line and the Wild-Type (WT) line in roots (n=3) and leaves (n=3). Legend: UT: The PP line; WT: WT line; F: leaves; R: Roots.

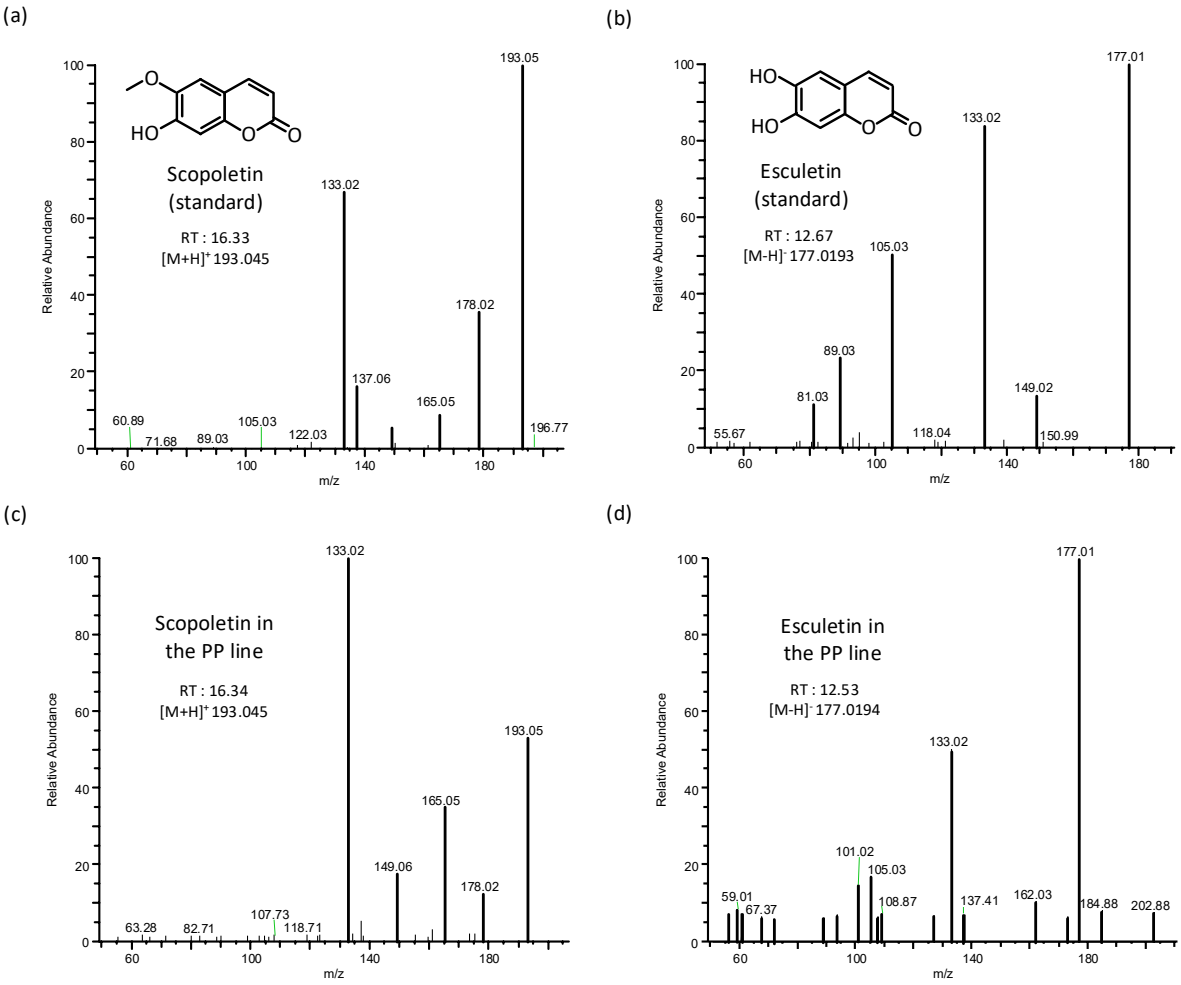

Figure S3: Formal identification of scopoletin and esculetin in the PP line. Tandem mass spectrometry fragmentation pattern of standards of (**a**) scopoletin and (**b**) esculetin and (**c**-**d**) their respective forms identified in the PP line. Analysis was performed after negative (for esculetin) or positive (for scopoletin) electrospray ionization (ESI) and Targeted Single Ion Monitoring (SIM) mode between 50 and 210 m/z. The Higher Energy Collisional Dissociation (HCD) fragmentation mode was investigated.